이학박사학위논문

Application of Recombinant Proteins as Alzheimer's disease Therapeutics and Protein Delivery Vehicle

알츠하이머 질병의 치료제 및 단백질 전달체로서

재조합 단백질의 응용

2018년 8월

서울대학교 대학원

화학부 생화학 전공

오재훈

Abstract

Therapeutic molecules such as small molecules (> 1 kDa) and gene are successfully achieved for various therapeutic researches. However, small molecules are resulted in off-target side effects due to its limited specificity and selectivity. Also, using genes as therapeutic molecules in many cases raises safety concerns while they used. Recombinant proteins should be alternative molecules for overcome those limitations. Recombinant proteins have several attractive features such as high specificity, selectivity, safety and the protein production process is very simple and systematic. Therefore, I used recombinant protein to apply on Alzheimer‘s Disease (AD) therapeutic and protein delivery vehicle.

AD is a neurodegeneration disorder that damages neurons and causes loss of brain functions that involve memory, learning and reasoning. There are two main pathological features of AD: intra-neuronal neurofibrillary tangles (NFTs) containing paired helical filaments (PHFs) comprised of hyper-phosphorylated tau and the accumulation of amyloid-β (Aβ) plaques in both intra- and extra-cellular neurons.

Accumulation of senile plaques is comprised of 40 or 42 length of hydrophobic amyloid-β peptides (Aβ1– 40 or Aβ1– 42). The type II membrane-bound zinc metallo-endopeptidase, NEP, is the key enzyme for degrading Aβ peptides. Because NEP is capable of degrade only monomer form of Aβ peptides but also oligomer form of Aβ peptide. In order to degrade neuronal toxic Aβ peptides, recombinant human soluble NEP protein which removed cell membrane bound region was produced by mammalian cells (HEK293T) to demonstrate protective effect against Aβ peptides in neuronal cells *in vitro*.

Neurofibrillary tangles (NFTs) are composed of aggregates of

hyperphosphorylated tau, which is a microtubule-associated protein. As a microtubule-associated protein, aggregates of normal tau protect cells against toxic hyperphosphorylation. Therefore, reducing the level of hyperphosphorylated tau is crucial for treating AD. In previous studies, heat shock proteins (HSPs) can bind with tau and Hsp27 which, especially, directly associates with hyperphosphorylated tau or PHF and eliminates tau aggregates. I investigated recombinant Hsp27 protein to obtain the protective effect on AD. To enhance the efficiency for delivering the protein, cell penetrating peptide called Tat was applied. HIV Tat is 11 amino acids sequence (YGRKKRRQRRR) that can be effectively internalized with the fused protein into the cells at reasonable concentration. After recombinant fusion Hsp27 protein was applied on neuronal cells, tau-induced neurodegeneration therapeutic effect had been demonstrated.

sNEP and Tat-Hsp27 recombinant proteins exhibited great potential as therapeutic molecules for AD.

The use of cell penetrating peptides (CPPs) applied on recombinant proteins facilitates great opportunities for various biomedical applications. However, high extracellular concentration threshold (micromolar level) at which showing significant penetration of CPPs fusion protein causes one of the crucial weaknesses impeding the broad biomedical applications.

In previous research, chemically synthesize 16 meric amphipathic α-helical LK peptide had been demonstrated enhancing effect of cell penetrating activity (nanomolar range) compared to conventional CPPs such as Tat or oligo-arginine. Furthermore, increased cell penetrating activity of LK peptide was obtained by multimerization. However, currently, with chemical synthesis could be elongated the peptide as only up to 50 amino acids. Therefore, recombinant protein technique should be better method for production of multimer form of LK peptide fusion proteins.

I produced momoneric LK to hexameric LK (LK-1 to LK-6) fusion proteins

in order to demonstrate the intracellular penetrating efficiency. The multimeric LK fused protein has demonstrated cell penetrating activity within a hundred nanomolar concentration which is about 100–1,000 fold lower concentrations than Tat-proteins. Interestingly, LK fusion proteins with monomer and multimer form underwent different penetration mechanism. The multimeric LK showed rapid cell penetration through macropinocytosis at low nanomolar concentrations, unlike the monomeric LK, which had slower penetrating kinetics at much higher concentrations. Mammalian cell membrane proteoglycan, heparin sulfate proteoglycan (HSPG), was seemed to be highly involved in the rapid penetration of multimeric fusion proteins. I delivered an adipogenic transcription factor, PPAR-γ2, into pre-adipocyte to demonstrate cell differentiation for biomedical applications.

It is essential to discover or develop new CPPs that are able to deliver proteins into cells at clinically feasible concentrations for future practical CPP fusion protein-based therapeutic applications.

Key words

Recombinant protein, Alzheimer's disease, Heat shock protein 27 (Hsp27), Neprilysin (NEP), Cell penetrating peptides (CPPs)

Student number: 2013-22928

Contents

Contents

List of figures

List of tables

Part A. Therapeutic Effect against Alzheimer's disease by using Engineered Recombinant Proteins Delivery.

Chapter 1. Protective Effect of Recombinant Soluble Neprilysin against β-amyloid Induced Neurotoxicity

Chapter 2. Protective Effect of Tat PTD-Hsp27 Fusion Protein on Tau Hyperphosphorylation Induced by Okadaic Acid in the Human Neuroblastoma Cell Line SH-SY5Y

Part B. Development of New Type of Cell-Penetrating Peptide Fusion Protein and Application for Transcription Control

Rapid Intracellular Protein Transport at Nanomolar Concentrations by Multimeric Amphipathic α-Helical Sequences

List of figures

Part A. Therapeutic Effect against Alzheimer's disease by using Engineered Recombinant Proteins Delivery.

Chapter 1. Protective Effect of Recombinant Soluble Neprilysin against β-amyloid Induced Neurotoxicity

Chapter 2. Protective Effect of Tat PTD-Hsp27 Fusion Protein on Tau Hyperphosphorylation Induced by Okadaic Acid in the Human Neuroblastoma Cell Line SH-SY5Y

Part B. Development of New Type of Cell-Penetrating Peptide Fusion Protein and Application for Transcription Control

Rapid Intracellular Protein Transport at Nanomolar Concentrations by Multimeric Amphipathic α-Helical Sequences

List of tables

Part B. Development of New Type of Cell-Penetrating Peptide Fusion Protein and Application for Transcription Control

Rapid Intracellular Protein Transport at Nanomolar Concentrations by Multimeric Amphipathic α-Helical Sequences

Part A. Therapeutic Effect against Alzheimer's disease by using Engineered Recombinant Proteins Delivery.

Chapter 1. Protective Effect of Recombinant Soluble Neprilysin against β-amyloid Induced Neurotoxicity

1. Abstract

The accumulation of amyloid beta (Aβ), a physiological peptide, in the brain shows strong evidence leading to the pathological cascade of Alzheimer's disease (AD). Therefore, regulation of Aβ represents a crucial treatment approach for AD. Neprilysin (NEP), a membrane metallo-endopeptidase, is a rate-limiting peptidase which is known to degrade the amyloid beta peptide. This study investigated soluble NEP (sNEP) produced by recombinant mammalian cells stably transfected with a non-viral NEP expression vector to demonstrate its protective effect against Aβ peptides in neuronal cells *in vitro*. Stably transfected HEK 293 cells were used to purify the soluble protein. sNEP and Aβ peptide co-treated hippocampal cells had a decreased level of Aβ peptides shown by an increase in cell viability and decrease in apoptosis measured by the CCK-8 and relative caspase-3 activity ratio assays, respectively. This study shows that stably transfected mammalian cells can produce soluble NEP proteins which could be used to protect against Aβ accumulation in AD and subsequently neuronal toxicity. Additionally, approaches using protein therapy for potential targets could change the pathological cascade of Alzheimer's disease.

2. Introduction

Alzheimer's disease (AD) is a neurodegeneration disorder that damages neurons and causes loss of brain functions that involve memory, learning and reasoning.[1] There are two main pathological features of AD: intra-neuronal neurofibrillary tangles (NFTs) containing paired helical filaments (PHFs) comprised of hyperphosphorylated tau [2] and accumulation of amyloid-β (Aβ) plaques in both intra- and extra-cellular neurons.[3] While previous studies have shown the role of tau in AD pathogenesis, this study focused on the amyloid cascade which leads to neuronal malfunction.

Senile plaques are mainly comprised of hydrophobic amyloid-β peptides which normally have a length of 40−42 amino acids (according to amino acids Aβ1−40 or Aβ1−42). Amyloid precursor protein (APP), which is cleaved by β-secretase and γ-secretase, produces Aβ.[4] The accumulation of Aβ1−40 and Aβ1−42 as long, unbranched fibril is a hallmark of AD as well as the loss of neurons due to cell death caused by the Aβ aggregation process.[3] In steady-state, Aβ is controlled by amyloid degrading enzymes and by perivascular drainage. However, perturbations in Aβ homeostasis that increase the steady-state levels of Aβ would thus be expected to increase the aggregation of Aβ into amyloid plaques.[5] These mechanisms become impaired with aging and disease such as AD.[6]

Neprilysin, a known neutral endopeptidase (NEP), is a 90-110 kDa type II membrane-bound zinc metallo-endopeptidase. NEP is comprised of an ectodomain, a transmembrane and short intracellular domain, which contains the catalytic site and belongs to the M13 family of proteases.[7] NEP is a potent endopeptidase that can directly degrade Aβ peptides which includes not only the monomer form but also the oligomer forms of Aβ. Thus, NEP has been identified as a critical Aβ degrading enzyme in the brain.[8] Reduction in the level of NEP was found to occur with aging leading to decreased Aβ clearance.[9] Thus,

considering the high levels of Aβ is a key factor when searching for potential therapeutic targets of AD.

In the present study, recombination human soluble NEP (sNEP) was produced by recombinant mammalian cells (HEK293T) with the pLEXm-NEP expression vector. The stable cell line continuously produced the protein in cell suspension conditions. The role of recombinant sNEP produced by mammalian cells was investigated for the treatment of AD *in-vitro*. These results support the potential use of recombinant sNEP as a protein therapeutic for the treatment of AD.

3. Materials and methods

3.1. Cell culture and media

Adherent condition for HEK 293T (human embryotic kidney) cell was purchased from the American Type Culture Collection (ATCC) and maintained in DMEM (high glucose) (Wellgene) plus 10% RBS (Wellgene) at 37 °C in 5% CO_2 incubator. And suspension condition for HEK 293T cell was maintained in suspension culture in shake flasks (100 - 130 rpm) in ex-cell 293 media (sigma) containing 6 mM L-glutamine and 1% FBS at 37 °C in 8% CO_2 incubator.

3.2. Construction of the expression vector

A gene encoding the extracellular domain (52-750) of human NEP (soluble human NEP) was produced by gene synthesis (Cosmo Genetech) and cloned into the vector pLEXm (Novagen). We designed a mammalian expression vector containing KOZAK sequence (GCCACC), gp64 signal peptide, hexahistidine tag and exclusion of trans-membrane domain sequence of human NEP. The extracellular hNEP fragment was generated by PCR using cDNA template and oligonucleotide primer NheI and XhoI restriction sites. The pLEXm vector and kozak, signal peptides and hexahistidine fragment were digested with KpnI and NdeI and ligated. The ligated vector was transformed into chemically competent DH5α E.coli strain (Enzynomics, Korea). After purification of the plasmid containing kozak, signal peptides and hexahistidine, the plasmid and the extracellular hNEP fragment were digested with NdeI and XhoI and ligated.

3.3. Establishing HEK293T-sNEP stable cell line

HEK 293T cells were seeded in a 6-well plate at a density of 7.5×10^5 cells/mL in DMEM containing 10% FBS medium. After 24 hours, the cells were washed twice with DPBS and then co-transfected by PAM R G4 (synthesis) using 5 μg

of pLEXm-sNEP and 0.5 μg of pcDNA 3.1 containing neomysin resistance. Co-transfection was stoped 48 h later by replacement with DMEM containing 5% FBS and 2 mg/mL Geneticin (Thermofisher) to select the transfected cells. Transfected cells were grown in 3 weeks to observe colony formed and media was changed every 2 days. After then, colonies were detached from the 6-well plate by trypsin-EDTA underwent limit dilution in 96-well plate and growing up to 6-well plate. Establishing the production of sNEP was detected by western blotting using mouse anti-human CD10 antibody (Abcam).

3.4. Stable expression of sNEP in the suspension system

HEK293T-sNEP, the cell stably expressed sNEP, was grown in T-75 flask (Falcon) contain DMEM (high glucose), 10% FBS at 37 °C, 5% CO_2. The cells fully grown, it detached with trypsin-EDTA and centrifuged 1300 rpm, 5 min to down the cells and re-suspended by Ex-cell 293 media contained 6 mM L-glutamine and 1% FBS. The cells were counted by heamatocytometer. Prior to harvesting, cells were expanded in 0.1 to 3 L Erlenmeyer flask. 5.0×10^5 cells/mL in 40 ml Ex-cell 293 media containing 1% FBS were seeded into the 100 ml Erlenmeyer flask (Corning). The cells were stirred in 120 rpm and grew 37 °C, 8% CO_2. The cells were grown every 2 days up to 1.5×10^6 cells/ml. For harvesting, 1.5×10^6 cells/mL in 1 L Ex-cell 293 media containing 1 % FBS lowered the temperature to 32 °C and the cells were grown in 5 days for expression.

3.5. Scaled-up expression

Large-scale expression (3 L) was performed using HEK 293T cells in suspension culture. The cells were harvested by centrifugation (6000 rpm, 20 min, 4 °C) and was applied to a HisTrap column (GE heathcare). Bound protein was eluted using buffer containing 20 mM Tris-HCl pH7.5, 500 mM NaCl, 1M imidazole. The eluted sample was further purified by gel filtration in a HiLoad

16/600 Superdex 200 prep-grade column (GE Heathcare), equilibrated with buffer containing 20 mM Tris-HCl pH 7.5, 100 mM NaCl. Purified soluble human NEP was concentrated using an Amicon Ultra-10K centrifugal filter device (Millipore).

3.6. Aβ peptide preparation and degradation assay

Aβ peptide (1–40 and 1–42) was purchased from Anaspec, Inc. Both peptides were dissolved in PBS to make final concentration of 500 μM. Then Aβ peptide (1–40 and 1–42) solutions were incubated at 37 °C for 3 days to produce aggregated forms. For oligomer, Aβ peptides (1–40 and 1–42) were dissolved in cold hexafluoro-2-propanol, and incubate at room temperature for 1 h to establish oligomerization. Protein extracted from HEK 293T cells was incubated with Aβ peptides (1–40 and 1–42). 500 μM of Aβ peptides (1–40 and 1–42) were incubated with sNEP concentration of 50 μM and 100 μM in 72 h at 37 °C. Degradation of Aβ peptides were observed by western blotting.

3.7. Western blot analysis

To detect the expression of sNEP in vitro, cells which sNEP stably transfected in suspension were counted by heamatocytometer. 1.5×10^6 cells were centrifuged at 15,000 rpm 10 min at 4 °C, and then collected supernatant. Using an Amicon Ultra-10K centrifugal filter device (Millipore) to concentrate the samples to 20X. Concentrated supernatants were subjected to a 12% SDS-PAGE on 12% gradient Tris-acetate polyacrylamide gel, followed by electrophoretic transfer to a nitrocellulose membrane. After blocking in 5% skim milk/TBST (Tris-buffered saline and 0.1% Tween 20, pH 7.5), the membrane washed in 15 min three times. Subsequently, the membrane reacted with mouse anti-human CD10 antigen (CALLA) (1:1000, overnight at 4 °C) (Abcam Inc, Cambridge, MA) and a second goat anti mouse-IgG-HRP antibody (1:1000, 1 h) (Santa Cruz Biotech, USA). The membrane was washed again

with TBST three times for 15 min each, and protein signals were detected by ECL (Amersham Pharmacia Biotech, USA) exposed to X-ray film.

To detect Aβ degradation using sNEP in vitro, the mixture samples of Aβ peptides and sNEP were applied by SDS-PAGE on 12% gradient Tris-acetate polyacrylamide gel. Electrophoretic transfer to nitrocellulose membrane subsequently underwent and incubated overnight at 4 °C with primary antibody using mouse anti-human Aβ peptide (1:1000) (DE2B4, Santa Cruz Biotech, USA). Then membrane applied 1 h at room temperature using a second goat anti mouse-IgG-HRP antibody (1:1000, 1 h) (Santa Cruz Biotech, USA) and visualized by ECL exposed to x-ray film.

3.8. Cell viability assay

A cytotoxicity assay was performed using a Cell Counting Kit-8 (Dojindo, Korea). HT22 cells were plated in a 96-well plate at 3×10^3 in 100 μL of DMEM medium containing 10% FBS for 24 h. Then, growth media was replaced with fresh culture media (100 μl/well) containing 1% FBS and different concentration (10 μM and 50 μM) of Aβ peptides 1–40 and 1–42 oligomers for 6 h. Subsequently, 0.5 μM and 50 μM sNEP was added. After 48 h and 72 h incubation, 10 μL of CCK-8 solution was added, and the cells were incubated at 37 °C for 1 h. The absorbance at 450 nm was measured using a microplate reader (Molecular Device Co., Menlo Park, CA)

3.9. Apoptosis assay

The induction of apoptosis leads to an activation of caspase-3 using Caspase-3 assay Kit (Sigma). HT cells were seed 1×10^3 cells per well on 96-well plate and allowed to adhere for 24 h. Cells were then incubated for 48 h and 72 h in the absence (control), presence of Aβ peptides (1–40 and 1–42) 50 μM and Aβ peptides (1–40 and 1–42) 50 μM with 1 μM of sNEP. Subsequently, cells were trypsinised, cells were centrifuged at 1200 rpm for 5 min at 4 °C. Prior to

suspend the cell pellets in 20 μL of 1X lysis buffer, removed supernatant. Cells were incubated on ice for 20 min, then were centrifuged the lysed cells at 16,000 rpm for 15 min at 4 °C. The cytosolic supernatant fractions were incubated with the colormetric caspase-3 tetra-peptide-substrate N-acetyl-Asp-Glu-Val-Asp-p-nitroanilide (Sigma) at a final concentration of 20 μM. Cleavage of the caspase-3 substrate was determined by using the microplate reader (Molecular Device Co., Menlo Park, CA) at a wavelength of 405nm.

3.10. Statistical analysis

Statistical analysis was performed with the Statistical Package for the Social Sciences (SPSS, IBM Corporation, NY, USA). Statistical significance was determined by analysis of variance (ANOVA) with Tukey's HSD test and student's t test. All results are presented as the mean ± standard deviation, and statistical significance was considered at the 5% level.

4. Results and Discussion

The discovery of Aβ peptides, otherwise known as senile plaques, as extracellular deposits in the grey matter of the brain has led to understanding the basis of memory loss in AD. Aβ peptides cause synaptic dysfunctions. Accumulation of Aβ peptides is widely known to have a critical role in the pathology of AD. AD causes not only monomeric forms but also oligomeric forms of Aβ which have more toxicity.[10] Both peptides, Aβ 1–40 and 1–42, contribute to the development of AD. Therefore, it is important to decrease the level of Aβ peptides in the treatment of AD. There are several candidates for Aβ-degrading enzymes such as gelatinase A[11], gelatinase B[12], insulin-degrading enzyme (IDE)[13], neprilysin[14], endothelin-converting enzyme (ECE)-1[15] and cathepsin D.[16] Among those candidates, neprilysin is the most potent Aβ-degrading enzyme mainly due to the properties of the Aβ oligomers and monomers.[10] Several studies have shown that increasing NEP in transgenic mice can protect against Aβ accumulation.[17] Neuronal overexpression of NEP in amyloid precursor protein (APP) mutated transgenic mice improved memory performance in the Morris water maze test.[18] This improvement was associated with a decreased level of Aβ without affecting APP processing in the brain. Previous studies used virus expression systems for NEP to lower Aβ in the brain.[19] These methods have limitations including difficulty in production, possibility of inserted genes combining to activate oncogenes and inflammatory responses. Protein delivery, however, overcomes many of these disadvantages and also has several benefits which are greater systemic bioavailability and potential for repeat production. Other studies have already shown that NEP degrades monomeric Aβ peptides.[20] In this study, we focused on the efficacy of the protein therapeutic approach using sNEP to protect neuronal cells from the toxicity of Aβ peptides. Removing the transmembrane domain was one of the key features of our soluble NEP, resulting in a constitutively active protease

that degrades Aβ peptides. We demonstrated the potential of using a non-viral vector carrying the NEP gene to produce soluble protein from stably transfected mammalian cells in liquid culture.

4.1. Construction of a sNEP HEK293T stable cell line

The DNA sequence encoding the extracellular NEP fusion protein was cloned into the pLEXm vector containing a hexahistidine which can be cleaved by thrombin (Figure 1). A signal sequence from insect cells was fused to the vector in front of the hexahistidine to enable protein secretion of its catalytically extracellular domain into the media. HEK293T cells were co-transfected with pLEXm-sNEP and pcDNA3.1 containing neomycin which is described in the Materials and Methods. After incubation for 3 weeks, neomycin resistance colonies were selected from growth medium containing 2 mg/mL Geneticin (G418). Isolated neomycin resistance HEK293T cell colonies were collected with cloning rings from 96-well plates and expanded on 6-well plates. Western blot analysis was done for the neomycin resistance cells to identify which HEK293T cells were stably transfected with sNEP (Figure 2). Lane 2 shows a sufficient amount of sNEP with expected protein size (84 kDa), thus, those HEK293T cells stably transfected with sNEP were selected for all further applications. Prior to using the cells, genomic DNA extraction was done to confirm that the sNEP gene was integrated into the host cells. A large amount of sNEP is required for affinity tag purification; thus, the cells were transferred from plates into 1.5 L of growth media. Figure 3A shows the viable cell count of the liquid culture and Figure 3B shows viability of the cells over 50 days (passage 6 to 20). An initial seeding of 4.0×10^5 cells/mL reached about 1.7×10^6 cells/mL in 2 or 3 days, after which the medium was replaced with fresh medium. Cell viability was over 90% during culture conditions.

4.2. Purification of recombinant sNEP from mammalian cells

HEK293T cells stably transfected with sNEP were grown in a 3 L Erlenmeyer flask containing 1.5 L of media at 37 °C. After replacing the media with fresh culture media, the culture temperature was decreased to 34 °C to enhance the expression efficiency. Lowering the temperature is known to decrease the cell growth rate and to subsequently increase the protein expression level [21]. Figure 4A shows the growth rate for 5 days and Figure 4B shows viability of the cells. The viability started to decrease on day 4, and about 80% of the cells were still viable on day 5. Thus, the medium containing the human soluble NEP was harvested on day 5, and the sNEP was initially purified on a HiTrap Chelating HP column (Figure 5A). The fractions from the HiTrap chelating HP column were run a 12% SDS-PAGE gel (Figure 5B). Fractions 1−5 were collected for further purification. The eluted fractions 1−5 were purified by gel filtration on a HiLoad 16/600 Superdex 200 prep-grade column (Figure 5C). Western blot analysis was done to verify the expression of sNEP. The sNEP proteins in Fractions 1–5 had a molecular size of 84 kDa. After combining and concentrating Fractions 1–5, the final concentration of the recombinant sNEP from 1.5 L of culture was 1.5 μM in 1 mL. The concentrated sNEP was analyzed by western blot shown in (Figure 5D). Additionally, the total protein amount of each sample was determined with the Bradford assay.

4.3. Decrease in the Aβ oligomer level by recombinant human soluble NEP

Aβ peptides 1–40 and 1–42 were incubated at 37 °C for 2 weeks to convert the monomeric form to the oligomeric form. Next, the recombinant sNEP, purified from a liquid culture of stably transfected cells, was incubated with the oligomeric form of the Aβ peptides 1–40 and 1–42 for 72 h. Thus, 50 μM and 100 μM sNEP were reacted with 400 μM Aβ oligomers (peptide 1–40 and 1–42), respectively, in a 37 °C incubator. Western blot analysis was done for both reactions (Figure 6A and 6B). The Aβ peptides (1–40 and 1–42) were significantly decreased by 50 μM and 100 μM sNEP. Thus, oligomeric Aβ

peptides were effectively degraded by sNEP.

4.4. Protection against Aβ peptide toxicity by sNEP in cells

A cytotoxicity assay was done to determine whether sNEP could protect against cell death induced by Aβ peptides (Aβ 1–40 and 1–42). HT22 cells were incubated for 72 h in DMEM media containing 1% FBS with different concentrations oligomeric Aβ peptides (1–40 and 1–42) and sNEP (Figure 7A and 7B). The results show that there was an increase in cell viability shown by CCK-8 when the cells were treated with Aβ and sNEP compared to cells treated with Aβ alone. Especially, when cells were treated with 50 μM Aβ 1–40 for 72 h, viable cells decreased down to 47%. When the cells were treated with sNEP and 50 μM Aβ 1–40, cell viability increased about 1.93 folds. Moreover, the treatment of cells with sNEP and 50 μM Aβ 1–42 for 72 h increased the viable cells by about 1.7 folds. Cells treated only with sNEP showed no effect on cell viability. In addition, Aβ-induced cell death was examined with the Caspase-3-assay (Figure 8A and 8B). After treating cells with 50 μM Aβ1-40 or Aβ1-42, the relative caspase-3 activity ratio increased 1.5, 1.55 (48 h) or 1.65, 1.85 folds (72 h). This increase was prevented by the addition of 1 μM sNEP which decreased the relative caspase-3 activity ratio to 0.78, 0.7 (48 h) or 1.08, 0.84 folds (72 h).

5. Conclusion

This study showed that the oligomeric Aβ 1–40 and 1–42 peptides are degraded by our recombinant soluble NEP. Our results suggest that the removed trans-membrane domain of NEP from our sNEP may have a major role in the pathogenesis of AD. Furthermore, the use of recombinant soluble NEP produced by mammalian cells could be an effective way to reduce levels of Aβ *in vitro*. Stably expressed sNEP from mammalian cells for protein therapy could affect the development and progression of AD as well as prevent the onset of the disease. The expressed sNEP was functional degrading oligomeric Aβ 1–40 and 1–42 peptides. Also, treating hippocampal cells HT22 with sNEP enhanced their survival following exposure to oligomeric Aβ peptides (1–40 and 1–42) compared to the control and decreased Aβ-mediated apoptosis *in vitro*. Protein therapy could be essential approach as an alternative method to treat AD as well as provide new methods to unlock the mechanisms behind the pathogenesis of AD in future studies.

6. Reference

1. Selkoe, D. J., Alzheimer's disease: genes, proteins, and therapy. *Physiol Rev* **2001,** *81* (2), 741-66.

2. Kosik, K. S.; Shimura, H., Phosphorylated tau and the neurodegenerative foldopathies. *Biochim Biophys Acta* **2005,** *1739* (2-3), 298-310.

3. Selkoe, D. J., Alzheimer's disease is a synaptic failure. *Science* **2002,** *298* (5594), 789-791.

4. (a) Selkoe, D. J., Alzheimer's disease results from the cerebral accumulation and cytotoxicity of amyloid beta-protein. *J Alzheimers Dis* **2001,** *3* (1), 75-80; (b) Evin, G.; Weidemann, A., Biogenesis and metabolism of Alzheimer's disease Abeta amyloid peptides. *Peptides* **2002,** *23* (7), 1285-97.

5. Spencer, B.; Rockenstein, E.; Crews, L.; Marr, R.; Masliah, E., Novel strategies for Alzheimer's disease treatment. *Expert Opin Biol Th* **2007,** *7* (12), 1853-1867.

6. Carare, R. O.; Hawkes, C. A.; Weller, R. O.; Nicoll, J. A., Lymphatic drainage of the brain and the pathology of Alzheimer's disease. *J Anat* **2011,** *218* (4), 462-462.

7. Turner, A. J.; Isaac, R. E.; Coates, D., The neprilysin (NEP) family of zinc metalloendopeptidases: genomics and function. *Bioessays* **2001,** *23* (3), 261-269.

8. Shirotani, K.; Tsubuki, S.; Iwata, N.; Takaki, Y.; Harigaya, W.; Maruyama, K.; Kiryu-Seo, S.; Kiyama, H.; Iwata, H.; Tomita, T.; Iwatsubo, T.; Saido, T. C., Neprilysin degrades both amyloid beta peptides 1-40 and 1-42 most rapidly and efficiently among thiorphan- and phosphoramidon-sensitive endopeptidases. *Journal of Biological Chemistry* **2001,** *276* (24), 21895-21901.

9. Iwata, N.; Tsubuki, S.; Takaki, Y.; Shirotani, K.; Lu, B.; Gerard, N. P.; Gerard, C.; Hama, E.; Lee, H. J.; Saido, T. C., Metabolic regulation of brain A beta by neprilysin. *Science* **2001,** *292* (5521), 1550-1552.

10. Kanemitsu, H.; Tomiyama, T.; Mori, H., Human neprilysin is capable of degrading amyloid beta peptide not only in the monomeric form but also the pathological oligomeric form. *Neuroscience Letters* **2003,** *350* (2), 113-116.

11. Yamada, T.; Miyazaki, K.; Koshikawa, N.; Takahashi, M.; Akatsu, H.; Yamamoto, T., Selective Localization of Gelatinase-a, an Enzyme Degrading Beta-Amyloid Protein, in White-Matter Microglia and in Schwann-Cells. *Acta Neuropathol* **1995,** *89* (3), 199-203.

12. Lee, D. H.; Kang, K., Purification and characterization of human 92-kDa type IV collagenase (gelatinase B). *Exp Mol Med* **1996,** *28* (4), 161-165.

13. Chesneau, V.; Vekrellis, K.; Rosner, M. R.; Selkoe, D. J., Purified recombinant insulin-degrading enzyme degrades amyloid beta-protein but does not promote its oligomerization. *Biochemical Journal* **2000,** *351*, 509-516.

14. Howell, S.; Boileau, G.; Crine, P., Neutral Endopeptidase (Ec-3.4.24.11) - Constructed Molecular-Forms Show New Angles of an Old Enzyme. *Biochem Cell Biol* **1994,** *72* (3-4), 67-69.

15. Eckman, E. A.; Reed, D. K.; Eckman, C. B., Degradation of the Alzheimer's amyloid beta peptide by endothelin-converting enzyme. *Journal of Biological Chemistry* **2001,** *276* (27), 24540-24548.

16. Hamazaki, H., Cathepsin D is involved in the clearance of Alzheimer's beta-amyloid protein. *Febs Letters* **1996,** *396* (2-3), 139-142.

17. Leissring, M. A.; Farris, W.; Chang, A. Y.; Walsh, D. M.; Wu, X. N.; Sun, X. Y.; Frosch, M. P.; Selkoe, D. J., Enhanced proteolysis of beta-amyloid in APP transgenic mice prevents plaque formation, secondary pathology, and premature death. *Neuron* **2003,** *40* (6), 1087-1093.

18. Poirier, R.; Wolfer, D. P.; Welzl, H.; Tracy, J.; Galsworthy, M. J.; Nitsch, R. M.; Mohajeri, M. H., Neuronal neprilysin overexpression is associated with attenuation of A beta-related spatial memory deficit. *Neurobiol Dis* **2006,** *24* (3), 475-483.

19. (a) Hama, E.; Shirotani, K.; Masumoto, H.; Sekine-Aizawa, Y.; Aizawa, H.;

Saido, T. C., Clearance of extracellular and cell-associated amyloid beta peptide through viral expression of neprilysin in primary neurons. *J Biochem-Tokyo* **2001,** *130* (6), 721-726; (b) Richter, M.; Iwata, A.; Nyhuis, J.; Nitta, Y.; Miller, A. D.; Halbert, C. L.; Allen, M. D., Adeno-associated virus vector transduction of vascular smooth muscle cells in vivo. *Physiol Genomics* **2000,** *2* (3), 117-127; (c) Nishikawa, Y.; Iwata, A.; Katsumata, A.; Xuan, X. N.; Nagasawa, H.; Igarashi, I.; Fujisaki, K.; Otsuka, H.; Mikami, T., Expression of canine interferon-gamma by a recombinant vaccinia virus and its antiviral effect. *Virus Res* **2001,** *75* (2), 113-121; (d) Boukhvalova, M. S.; Yim, K. C.; Kuhn, K. H.; Hemming, J. P.; Prince, G. A.; Porter, D. D.; Blanco, J. C. G., Age-related differences in pulmonary cytokine response to respiratory syncytial virus infection: Modulation by anti-inflammatory and antiviral treatment. *J Infect Dis* **2007,** *195* (4), 511-518.

20. El-Amouri, S. S.; Zhu, H.; Yu, J.; Gage, F. H.; Verma, I. M.; Kindy, M. S., Neprilysin protects neurons against Abeta peptide toxicity. *Brain research* **2007,** *1152*, 191-200.

21. Lin, C. Y.; Huang, Z.; Wen, W.; Wu, A.; Wang, C. Z.; Niu, L., Enhancing Protein Expression in HEK-293 Cells by Lowering Culture Temperature. *Plos One* **2015,** *10* (4).

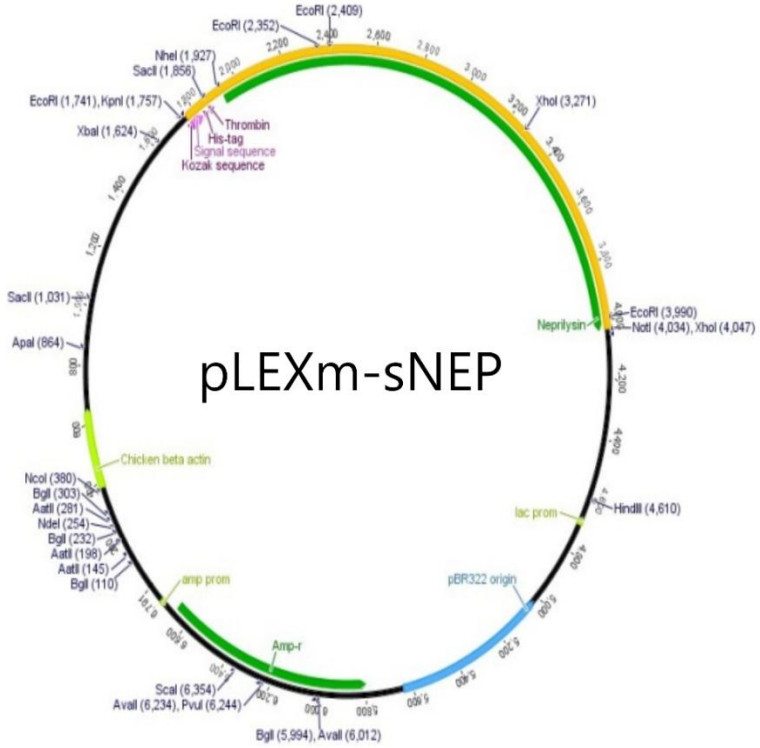

Figure 1. Construction of recombinant vector pLEXm-sNEP.

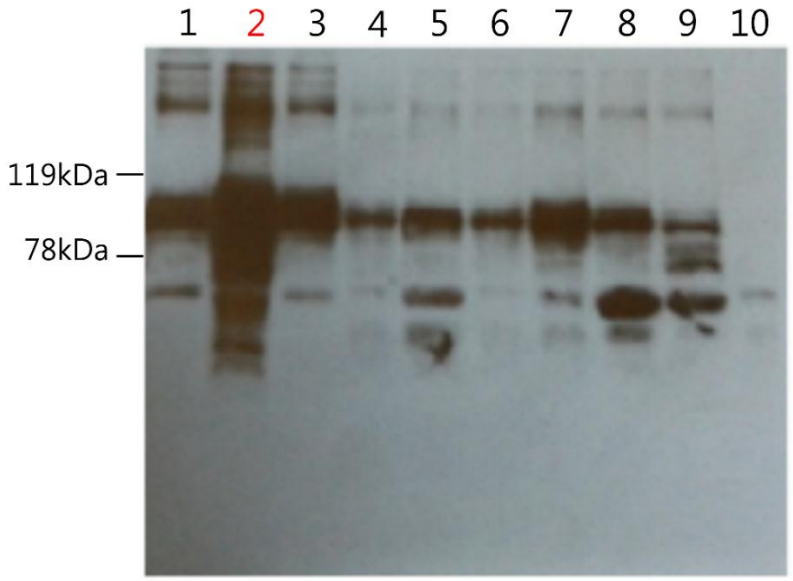

Figure 2. Western blot was performed on samples in different stable transfection colonies.

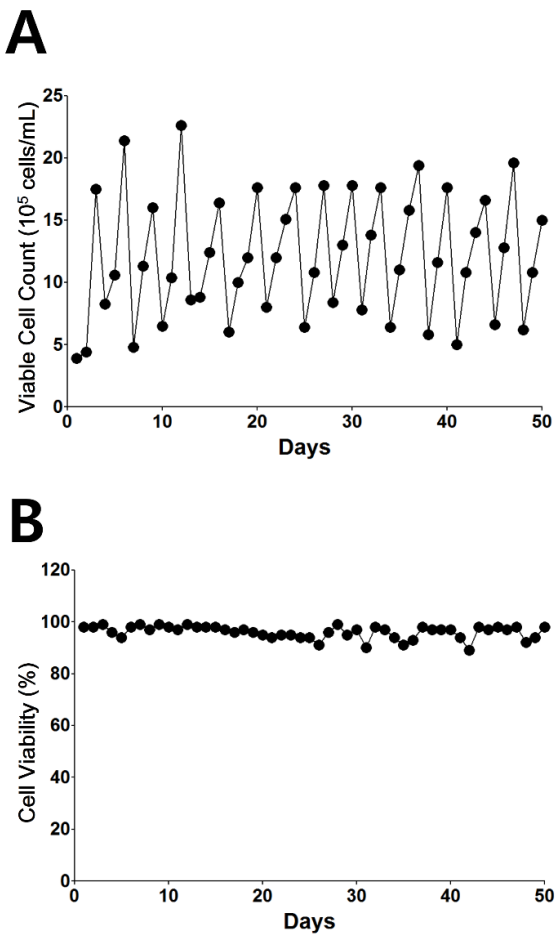

Figure 3 Suspension culture of sNEP stably transfected HEK293T cells viable cell count and viability over 50 days. A) Viable cell count of the suspension culture. B) Cell viability of suspension culture over 50 days.

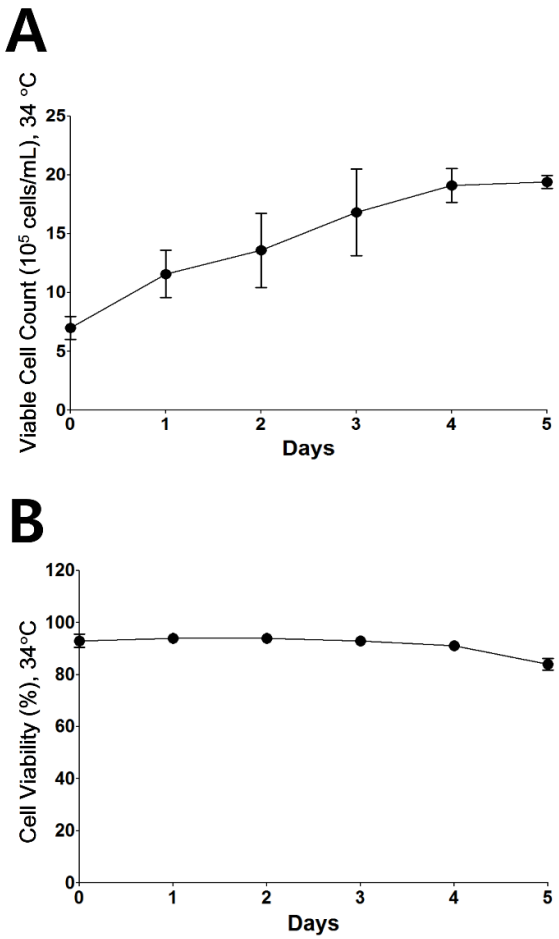

Figure 4. Suspension culture of sNEP stably transfected HEK293T cells viable cell count and viability. A) Viable cell count over 5 days at 34 °C. B) Cell viability at 34 °C. All data points are represented as the average value of three experiments ± standard deviation.

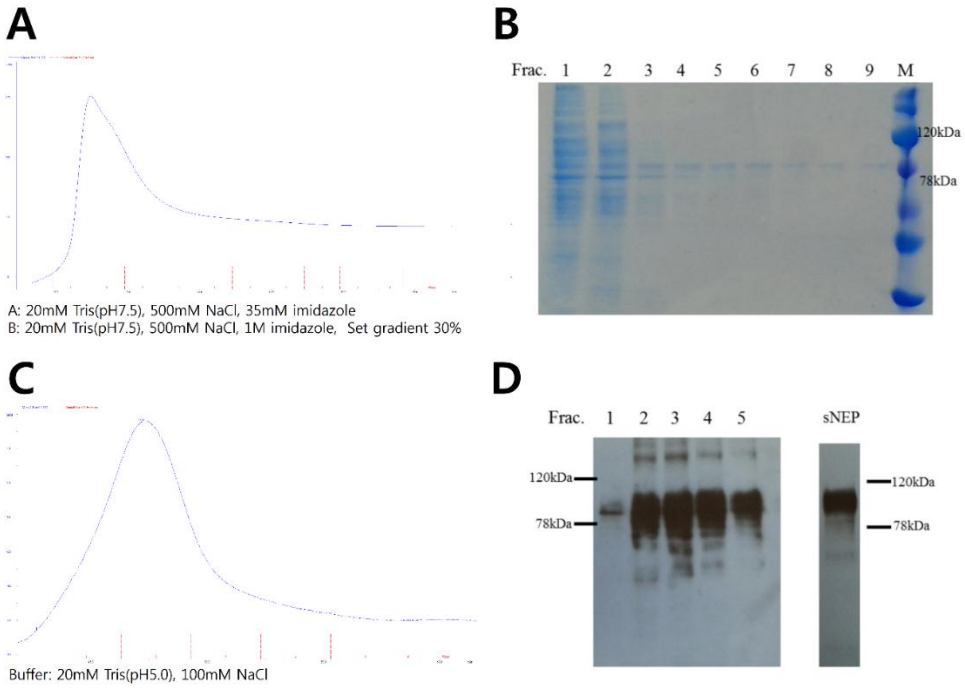

Figure 5. Human soluble NEP purification. A) The HiTrap Chelating HP column bound protein eluted with buffer (20 mM Tris-HCl pH 7.5, 500 mM NaCl, 1M Imidazole). Flow rate: 5 mL/min. B) SDS-PAGE was performed using HiTrap. Fraction 1–5 showed high affinity for the His-tag column. C) Superdex 200 column was eluted with buffer (20 mM Tis-HCl, 100 mM NaCl). Flow rate: 1 mL/min. D) Fractions were analyzed using western blot analysis after size exclusion chromatography step. Concentrated sNEP (10 μM) was also performed on western blot analysis using anti-human CD10 antigen.

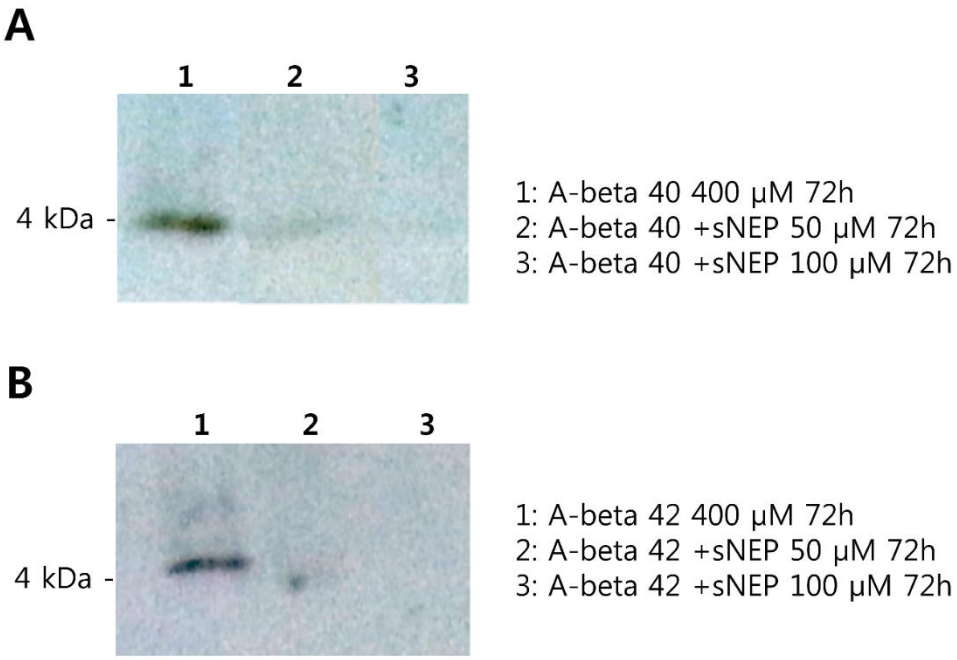

Figure 6. Aβ degradation assay was performed by western blot. A) 400 µM Aβ1–40 reacted with 50 µM or 100 µM sNEP, respectively. B) 400 µM Aβ1–42 reacted with 50 µM or 100 µM sNEP, respectively. Both Aβ peptides were efficiently degraded by sNEP.

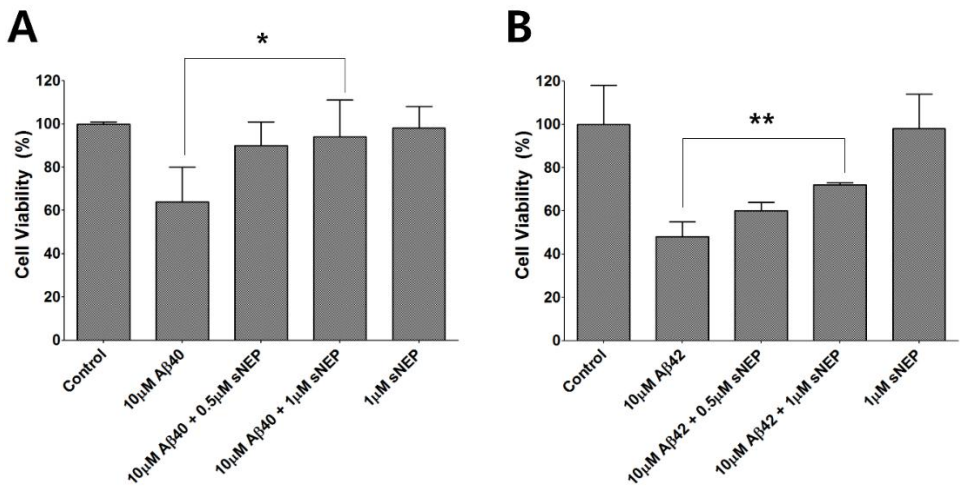

Figure 7. Aβ induced HT22 cells were protected by sNEP. Protective effects of sNEP on cell viability against induced cytotoxicity in HT22 cell line. Cell viability was increased in 10 μM of Aβ; A) Aβ 40, B) Aβ 42 with 1 μM of sNEP treat after 72 h. *$p < 0.05$ compared with the control. **$p < 0.05$ compared with Ab alone. All data points are represented as the average value of three experiments ± standard deviation.

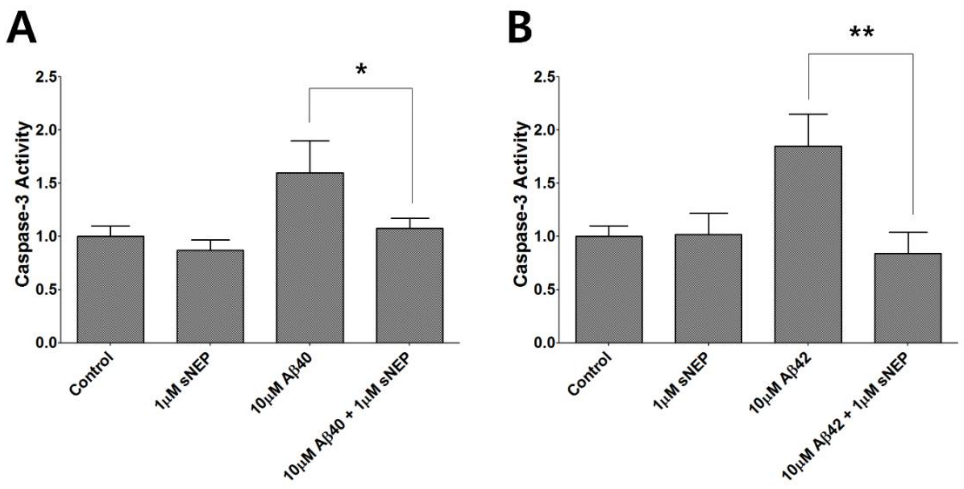

Figure 8. Aβ induced HT22 cells were protected by sNEP. Relative caspase-3 activity ratio against positive control. 10 μM of Aβ; A) Aβ 40, B) Aβ 42 was treated with 1 μM sNEP. This demonstrated that apoptotic cells by Aβ were decreased by treatment with sNEP. *$p < 0.05$ compared with the control. **$p < 0.05$ compared with Ab alone. All data points are represented as the average value of three experiments ± standard deviation.

Chapter 2. Protective Effect of Tat PTD-Hsp27 Fusion Protein on Tau Hyperphosphorylation Induced by Okadaic Acid in the Human Neuroblastoma Cell Line SH-SY5Y

1. Abstract

Alzheimer's disease (AD) is an age-related disorder that causes a loss of brain function. Hyperphosphorylation of tau and the subsequent formation of intracellular neurofibrillary tangles (NFTs) are implicated in the pathogenesis of AD. Hyperphosphorylated tau accumulates into insoluble paired helical filaments that aggregate into NFTs; therefore, regulation of tau phosphorylation represents an important treatment approach for AD. Heat shock protein 27 (Hsp27) plays a specific role in human neurodegenerative diseases; however, few studies have examined its therapeutic effect. In this study, we induced tau hyperphosphorylation using okadaic acid, which is a protein phosphatase inhibitor, and generated a fusion protein of Hsp27 and the protein transduction domain of the HIV Tat protein (Tat-Hsp27) to enhance the delivery of Hsp27. We treated Tat-Hsp27 to SH-SY5Y neuroblastoma cells for 2 h; the transduction level was proportional to the Tathsp27 concentration. Additionally, Tat-Hsp27 reduced the level of hyperphosphorylated tau and protected cells from apoptotic cell death caused by abnormal tau aggregates. These results reveal that Hsp27 represents a valuable protein therapeutic for AD.

2. Introduction

Alzheimer's disease (AD) is a progressive neurological disorder that causes memory loss. Various pathological hallmarks of AD include synaptic and neuronal loss, amyloid plaques primarily composed of the 42-residue hydrophobic b-amyloid peptide (Aβ)[1], and neurofibrillary tangles (NFTs) composed of aggregates of hyperphosphorylated tau, which is a microtubule-associated protein.[2] Amyloid plaques and NFTs are considered as the primary factors involved in the pathogenesis of AD.[3] Although previous studies have primarily focused on the role of β-amyloid peptides, recent studies on the role of tau in AD pathogenesis have indicated that hyperphosphorylated tau aggregates into insoluble paired helical filaments (PHFs), which induce neuronal dysfunction.[4] Moreover, these two pathological hallmarks demonstrate synergistic effects on synaptic dysfunction.[5, 6] As a microtubule-associated protein, aggregates of normal tau protect cells against toxic hyperphosphorylation, although neuronal death occurred following a period of survival.[7] However, tau is not only abnormally phosphorylated but also aggregates into insoluble forms such as PHFs and NFTs[8] in various AD mouse models.[9] Therefore, an approach that reduces the level of hyperphosphorylated tau would represent a valuable treatment for AD.[10] Tau can bind heat shock proteins (Hsps), which trigger the recruitment of CHIP (which is a co-chaperone that exhibits E3 activity), to the complex. CHIP has been shown to interact with tau, appears to work in concert with both Hsp70 and Hsp90 in degrading toxic tau species.[11] CHIP induces the ubiquitination of tau and activates its degradation when tau is defective.[12] In addition, The BAG2/Hsp70 complex is tethered to the microtubule and this complex can capture and deliver Tau to the proteasome for ubiquitin-independent degradation.[13] Curcumin also downregulated the levels of phosphorylated tau, which may be potentially attributed to the curcumin-induced upregulation in BAG2 levels in the

neurons.[14] Hsp27 directly associates with hyperphosphorylated tau or PHFs and regulates cell survival by eliminating tau aggregates.[15a] Heat shock proteins are induced in response to cellular stress as molecular chaperones that inhibit protein aggregation.[16] HSPs can prevent apoptosis and increase cell viability during cellular stress.[15a, 17] HSPs are also critical regulators of normal neural physiological function and cell stress responses.[18-20] However, the therapeutic effects of exogenous Hsp27 on disease models have not been investigated. Therefore, in this study, we investigated whether Hsp27 could reduce hyperphosphorylated tau in AD-induced SH-SY5Y cells. To more effectively deliver Hsp27 into cells, we combined the HIV protein transduction domain (PTD) Tat with the Hsp27 protein (Tat-Hsp27). HIV Tat (11 residues, YGRKKRRQRRR) can rapidly transduce into cells[21] and deliver full-length proteins into cells.[22] Tat-Hsp27 effectively reduced the phosphorylation of tau and rescued the cell death caused by abnormal tau aggregates. Therefore, our study suggests that Tat-Hsp27 may represent a potential protein therapeutic for tau-induced neurodegeneration.

3. Materials and Methods

3.1. Construction of the expression vector

We designed a bacterial expression vector (6X His-Tat-Hsp27) containing hexahistidine leader sequence, 11-amino acid Tat PTD sequence (YGRKKRRQRRR), and Hsp27 protein sequence. The Hsp27 fragment (BD Bioscience) was generated by PCR using human cDNA as a template and oligonucleotide primers containing BamHI and XhoI restriction sites. The pET-28a vector (Novagen) and the Tat PTD were digested with NdeI and BamHI and ligated. The ligated vector was transformed into chemically competent DH5a E. coli cells (Enzynomics, Korea). After purification of the plasmid containing the Tat PTD, the plasmid and the Hsp27 fragment were digested with BamHI and XhoI and ligated. We also designed pET28a vector containing Hsp27 (wt-Hsp27) genetically fused with a hexahistidine (His6) tag. The plasmid was constructed by digesting the pET28a vector with BamHI and XhoI restriction endonucleases and ligating the Hsp27 fragment digested with the same restriction enzymes into the cut vector. The recombinant plasmids (pET28a-Tat-Hsp27, pET28a-Hsp27) were transformed into the Escherichia coli strain BL21 (DE3) for protein expression (Enzynomics, Korea).

3.2. Expression and purification of Hsp27

The recombinant plasmid (6X His-Tat-Hsp27) was transformed into the E. coli strain BL21 (DE3) for protein expression. Transformed cells were plated on an LB agar (Merck) plate containing kanamycin (Sigma) and incubated overnight at 37 °C. Two-hundred milliliters of LB medium containing 1 mM kanamycin was inoculated with a single colony and incubated overnight at 37 °C with shaking at 200 rpm. The following day, 1 L of LB medium was inoculated with this preculture and incubated at 37 °C until an OD 600 of 0.5 was reached. Protein expression was induced by the addition of Isopropyl b-D-1-

thiogalactopyranoside (MB cell, Korea) at a final concentration of 1 mM, and the cells were incubated at 37 °C for an additional 4 h. The cells were centrifuged at 6000 rpm for 15 min at 4 ºC and resuspended in binding buffer (20 mM Tris-HCl, 500 mM NaCl, 35 mM imidazole, pH 7.5). Cells were lysed by sonication on ice using a sonicator (Sonics Vibra-Cell VCX 750, Sonic & Materials Inc., USA) with 1-s pulses and 8-s pauses for 30 min. After sonication, the lysates were centrifuged at 10,000 rpm for 15 min. The clarified lysate was loaded onto a pre-equilibrated HisTrap HP column (GE Healthcare). His-tagged Tat-Hsp27 protein was eluted with elution buffer (20 mM Tris-HCl, 500 mM NaCl, 1 M imidazole, pH 7.5). His-tagged Tat-Hsp27 was further purified using size exclusion chromatography on a HiLoad 16/600 Superdex 200 prep grade column (GE Healthcare) using 20 mM Tris-HCl (pH 7.5) and 100 mM NaCl. Wt-Hsp27 purification was performed in the same manner as in the purification step above. For the detection of Tat-Hsp27 delivery into cells, we conjugated FITC to Tat-Hsp27 using an FITC labeling kit (Thermo Scientific). The concentration of protein was determined using BCA protein assay kit (Pierce).

3.3. Labeling of wt-Hsp27, Tat-Hsp27

To eliminate any primary amines or ammonium ions from previous buffer, the buffers for both wt-Hsp27 and Tat-Hsp27 were exchanged with 50 mM sodium borate of pH 8.5 using Amicon ultra centrifugal filters. Two-hundred thirty micrograms of the prepared protein was added to a vial of FITC Reagent (50 μg). The reaction mixture was incubated for 60 min at room temperature protected from light. After adding the mixtures to the spin columns, they were centrifuged to remove any excess FITC at 15000 rpm for 1 min.

3.4. Cell culture

SH-SY5Y human neuroblastoma cells were grown in Roswell Park Memorial

Institute 1640 medium supplemented with 10% fetal bovine serum and 1% antibiotic–antimycotic under an atmosphere of 5% CO2 and 95% air (all from WELGENE). The medium was refreshed every three days. Cells below passage 24 were used for experiments. We chose the SH-SY5Y cell line because these human neuroblastoma cells express constantly endogenous tau.

3.5. Western blot analysis

For Western blot analysis, the cells treated with Tat-Hsp27 and okadaic acid were washed in DPBS and harvested in RIPA buffer (Pierce). To prevent from further phosphorylation, we added Protease inhibitor cocktail and phosphatase inhibitor cocktail composed of sodium orthovanadate, sodium molybdate, sodium tartrate, and imidazole (both from Sigma-Aldrich) into the cell lysates. Lysates were then centrifuged at 15,000 rpm for 15 min at 4 °C. The supernatant was separated in a 12% SDS-PAGE gel, and the proteins were transferred to a nitrocellulose membrane. After blocking in 5% skim milk/TBST (Trisbuffered saline and 0.1% Tween 20, pH 7.5), the membrane was washed in TBST three times (15 min each) and incubated with primary antibody overnight at 4 °C. The membrane was subsequently washed and incubated with the appropriate secondary antibody (HRP-conjugated goat antimouse and goat anti-rabbit) for 2 h at room temperature. Protein signals were developed with ECL Western Blotting Detection Reagent (Amersham Pharmacia Biotech, Piscataway, NJ, USA) exposed to X-ray film. Band intensities were calculated with the Image J software, and the protein band of interest was normalized to b-actin. Then, tau hyperphosphorylation was normalized to the total tau as a ratio, pTau/Total tau. Peroxidase-linked anti-rabbit and anti-mouse IgGs were purchased from Santa Cruz Biotechnology (USA). Rabbit polyclonal anti-tauphosphoserine 199/202 antibody and mouse monoclonal anti-tau-1 antibody were obtained from Millipore (USA). Anti-human total tau monoclonal antibody (HT 7), rabbit anti-Hsp27 polyclonal antibody, and anti Phospho-PHF-tau (detected phospho-

S202, -T205) monoclonal antibody (AT 8) were purchased from Pierce Biotechnology (USA). Anti-HIV1 tat monoclonal antibody was purchased from Abcam (USA). Synthesized tat peptides (YGRKKRRQRRR) were purchased from PEPTRON (Korea).

3.6. Immunocytochemistry

The SH-SY5Y cells were seeded on 2-well slides (Lab-Tek chamber, Nalge Nunc, NY) at a density of 5.0×10^5 per well, treated with 2 μM Tat-Hsp27 for 2 h, and then treated with 10 nM okadaic acid for 14 h. The cells were rinsed two times with PBS and fixed with 4% paraformaldehyde for 30 min. The cells were subsequently permeabilized for 10 min with 0.5% Triton X-100 followed by three 5-min washes in PBS. To reduce nonspecific binding, we used PBS containing 0.5% bovine serum albumin as blocking buffer. After incubation with the blocking buffer for 1 h, the cells were incubated with the primary antibody AT8 (anti Phospho-PHF-tau detected phospho-S202, -T205) for 4 h, followed by three 5 min washes. The cells were subsequently incubated with goat anti-rabbit (H + L) FITC conjugated antibody. After washing with PBS, cells were imaged using an image restoration microscope (Applied Precision, USA).

3.7. Cell viability/cytotoxicity assay

A cytotoxicity assay was performed using a Cell Counting Kit-8 (Dojindo, Korea). SH-SY5Y cells were plated in a 96-well plate at 5.0×10^4 in 100 μL of RPMI 1640 medium containing 10% FBS. After incubation for 48 h, cells were treated with 0.5 μM or 2 μM Tat-Hsp27 for 2 h. Subsequently, 10 nM and 50 nM okadaic acid were added for 6 h to induce abnormally phosphorylated tau. Ten microliters of CCK-8 solution was added, and the cells were incubated at 37 °C for 2 h. The absorbance at 450 nm was measured using a microplate reader (Molecular Devices Co., Menlo Park, CA).

3.8. In situ terminal deoxynucleotidyl transferase dUTP nick-end labeling (TUNEL) assay

SH-SY5Y cells were seeded on a 2-well slide at a density of 5.0×10^5 per well, treated with 2 μM Tat-Hsp27 for 2 h, and then treated with 10 nM okadaic acid for 14 h. The cells were fixed by immersion in PBS containing 4% formaldehyde (pH 7.4). After washing with PBS, the cellswere permeabilized in 0.2% Triton X-100 and washed again. After treatment with equilibration buffer, the cells were added to rTdT incubation buffer containing nucleotide mix. To terminate the reaction, saline sodium citrate buffer was added to the cells; nuclei were stained with DAPI and the mounting media used was Vectashield. The cells were analyzed under a fluorescence microscope at 520 nm (green fluorescence) and 460 nm (blue, DAPI).

3.9. Statistical analysis

Statistical analysis was performed with the Statistical Package for the Social Sciences (SPSS, IBM Corporation, NY, USA). Statistical significance was determined by analysis of variance (ANOVA) with Tukey's HSD test and student's t test. All results are presented as the mean ± standard deviation, and statistical significance was considered at the 5% level.

4. Results and Discussion

In this study, the recombinant Tat-Hsp27 reduced the level of hyperphosphorylated tau induced by okadaic acid in SHSY5Y neuroblastoma cells and prevented the apoptosis induced by abnormal tau aggregates in our cellular model of AD. The effect of Hsp27 on phosphorylated tau has recently received increasing attention. However, fewstudies have examined the therapeutic effect of Hsp27 on hyperphosphorylated tau, which has been implicated in the pathogenesis of AD. We demonstrate that Hsp27 exhibits a protective effect on apoptotic cell death caused by pathological tau. This finding suggests that Hsp27 may represent a potential protein therapeutic for AD. Tau stabilizes microtubules; however, tau mutations that result in its hyperphosphorylation lead to the formation of tau filaments that can form twisted ribbons or rope-like filaments.[2] Using phosphorylation-dependent monoclonal antibodies against tau, mass spectrometry, and sequencing, at least thirty phosphorylation sites have been reported.[10] Because the phosphorylation of tau is regulated by various kinases, including proline-directed protein kinases andglycogen synthase kinase 3, and phosphatases, including Ser/Thr protein phosphatases 1, 2A, 2B (calcineurin) and 2C, we used okadaic acid, which is a protein phosphatase inhibitor, to induce PHF-like hyperphosphorylation of tau.[23] Hsp27 facilitates the degradation and prevents the aggregation of aberrant substrates independent of ATP or ubiquitination.[15, 24] The mechanism by which Hsp27 prevents apoptosis could be from not only the interaction between Hsp27 and the pathologically hyperphosphorylated tau but also from Hsp27-mediated inhibition of procaspase-9 and caspase-3.[25] PP2A dephosphorylates Hsp27 more effectively than that of PP1, which is weakly active. Many of the sites that are dephosphorylated by PP2A are phosphorylated by either GSK-3b or Cdk5. These include S199, S202, T205, S396, and S404 93–96. We used the AT8 antibody to detect phosphorylated tau at Ser202 and Thr205.[26] Okadaic

acid inhibits Ser/Thr protein phosphatases and can induce tau hyperphosphorylation and neurodegeneration.[27] A recent study reported that hyperphosphorylation of tau leads to a 20-fold inhibition of the tau–tubulin binding affinity. This finding supports the critical role for tau in the pathogenesis of NFT-induced degeneration because the balance between kinases and phosphatases is disturbed in AD, resulting in the disassociation of tau from microtubules and its subsequent aggregation.[28] In our previous study, we showed that hyperphosphorylated tau, but not the overexpression of normal tau alone, reduces the cell viability of the neuroblastoma cell line SH-SY5Y.[29] Thus, in the present study, a cellular model of AD was induced by the hyperphosphorylation of endogenous tau. Moreover, we utilized the PTD of the HIV Tat protein to enhance the delivery of Hsp27, thereby enhancing its protective effect.[18, 30] Conjugation with specific peptide sequences, which are termed PTDs or cell-penetrating peptides, improves the delivery of a range of agents, including antisense oligonucleotides, plasmids, microbeads, and liposomes, which suggests that these peptide sequences may represent a universal in vitro and in vivo cellular delivery system.[22] To determine whether Tat-Hsp27 has aprotective effect against okadaic acid-induced cell death, SH-SY5Y cells containing hyperphosphorylated tau were treated with the fusion protein. The levels of phosphorylated tau significantly decreased compared with the cells that were not treated with Tat-Hsp27, and the relative cell viability was enhanced. This result suggests that Tat-Hsp27 represents a potential protein therapeutic to reduce hyperphosphorylated tau. Protein delivery systems offer several advantages, such as the ease of production from synthetic or natural compounds which provoke low inflammatory response.[31] Compared to other delivery systems, such as gene delivery utilizing plasmids or viral vectors, our recombinant Tat-Hsp27 has several advantages. The straightforward purification of Tat-Hsp27 is amenable to large-scale production. Moreover, Tat-Hsp27 is nontoxic and stable and can be readily delivered into

cells.

4.1. Purification of Hsp27 and Tat-Hsp27

The sequence encoding Tat-Hsp27 fusion protein was cloned into the pET28a vector (Figure 1), which produces a recombinant protein with a hexahistidine tag and purified using affinity purification and size exclusion chromatography. Fractions containing His-tagged Tat-Hsp27 were identified using 12% SDS-PAGE analysis with Coomassie Brilliant Blue staining. His-tagged Tat-Hsp27 in fractions 1–6 exhibited high affinity for the affinity matrix (Figure 2A). The eluted His-tagged Tat-Hsp27 was further purified using size exclusion chromatography (Figure 2B). Fractions containing His-tagged Tat-Hsp27 were identified using 12% SDS-PAGE with Coomassie Brilliant Blue staining. His-tagged Tat-Hsp27 eluted as a single peak from size exclusion chromatography, as confirmed by Western blot analysis (Figure 3), and migrated to a position slightly above the 25 kDa molecular weight marker in 12% SDS-PAGE analysis. The purified recombinant His-tagged wt-Hsp27 and Tat-Hsp27 was concentrated to 5.85 and 1.438 mg/mL as determined using the BCA assay, respectively.

4.2. Identification of Tat-Hsp27 cell penetration

To investigate whether Tat-Hsp27 could be effectively delivered into cells, we conjugated FITC to Tat-Hsp27. Image restoration microscopy indicated that FITC-Tat-Hsp27 was efficiently delivered into SH-SY5Y cells following treatment for 2 h at a concentration of 2 μM, in contrast to 2 μM wt-Hsp27 (Figure 4). We also performed Western blot analysis to confirm the intracellular delivery of Tat- Hsp27 and to determine whether its transduction is dependent on the Tat-Hsp27 concentration. SH-SY5Y cells were treated with Tat-Hsp27 for 2 h and were lysed using RIPA buffer. As shown in Figure 5, Hsp27 was present in the lysate of SH-SY5Y cells treated with 2 and 5 μM Tat-Hsp27,

whereas equivalent concentrations of wt-Hsp27 did not transduce cells. Additionally, increasing the concentration of Tat-Hsp27 used to treat cells resulted in an increased level of delivered protein. Therefore, the recombinant Tat-Hsp27 can be delivered into cells in a concentration-dependent manner.

4.3. Tat-Hsp27 protective effect on hyperphosphorylated tau

Because Hsp27 is known to have an effect on phosphorylation, we investigated whether Hsp27 can reduce the level of hyperphosphorylated tau, which is implicated in the pathogenesis of AD. Figure 6 demonstrated the schedule to see the protective effect on hyperphosphorylated tau. SH-SY5Y cells were treated with 2 or 5 μM Tat-Hsp27 for 2 h, and the phosphorylation of normal tau was induced by the addition of 50 or 100 nM okadaic acid. To quantify the relative phosphorylation, we normalized the level of hyperphosphorylated tau (p-tau) in Western blot analysis to the level of total tau using SigmaPlot software. Following treatment with 50 or 100 nM okadaic acid for 2 h, the level of hyperphosphorylated tau was approximately 2.4-fold or three-fold greater than the control group, respectively. Following treatment with 50 nM okadaic acid, the level of p-tau in cells pretreated with 2 and 5 μM Tat-Hsp27 decreased with an increasing concentration of Tat-Hsp27 (Figure 7), whereas equivalent concentration of tat peptide did not prevent tau hyperphosphorylation and oligomers (Figure 8). Tat-Hsp27 did not revert tau phosphorylation and aggregation into oligomers when added at the same time or after okadaic acid (as data not shown). Following treatment with 100 nM okadaic acid, cells pretreated with 5 μM Tat-Hsp27 showed slightly higher levels of p-tau than cells pretreated with 2 μM Tat-Hsp27. This finding suggest that when tau is hyperphosphorylated, the protective effect was better 2 than 5 μM Tat-Hsp27 on the reduction in hyperphosphorylated tau. Therefore, we used 2 μM Tat-Hsp27 in subsequent experiments. We also performed immunocytochemistry using an anti-p-tau antibody conjugated to FITC (Figure

9A). SH-SY5Y cells were treated with 2 μM Tat-Hsp27 for 2 h and were subsequently treated with 10 nM okadaic acid for 14 h. The level of p-tau was significantly decreased compared with treatment with okadaic acid alone (n = 3) (Figure 9B).

4.4. Protection cell against hyperphosphorylated tau toxicity by Tat-Hsp27 in cells

A cytotoxicity assay was performed to determine whether Tat-Hsp27 directly affected the cell death induced by hyperphosphorylated tau. We first evaluated the relative cell viability (RCV) in the presence of Tat-Hsp27 alone. As shown in Figure 10A, treatment with Tat-Hsp27 alone did not alter the RCV of normal cells. In contrast, SH-SY5Y cells treated with 10 and 50 nM okadaic acid for 6 h exhibited a decrease in 70, 49% cell viability (*$p < 0.05$). When cells were treated with 0.5 or 2 μM Tat-Hsp27 followed by treatment with 10 and 50 nM okadaic acid, the cell viability increased to 92, 90, 77, and 82%, respectively (**$p < 0.01$; Figure 10B). Cells treated with 0.5 and 2 μM Tat-Hsp27 clearly showed a protective effect against cell death induced by hyperphosphorylated tau. Treatment with 10 nM okadaic acid alone for 14 h greatly increased the number of TUNEL-positive cells, whereas the cells pretreated with 2 μM Tat-Hsp27 exhibited decreased TUNEL positivity (Figure 11). In the control group, apoptotic cells comprised 2% of the total number of cells. Following exposure to 10 nM okadaicacid, the percentage of apoptotic cells increased to 18%. However, this increase was inhibited by Tat-Hsp27 (5%). Therefore, intracellular delivery of Tat-Hsp27 prevented the apoptotic cell death induced by hyperphosphorylated tau.

5. Conclusion

We utilized the PTD of the HIV Tat protein to enhance the delivery of Hsp27, thereby enhancing its protective effect. Then, we designed a recombinant Tat-Hsp27 fusion protein to treat a cellular AD model, and this fusion protein was delivered into cells at high levels within 2 h. As previously mentioned, PTDs can readily and rapidly deliver proteins into cells. We confirmed that the fusion protein of Hsp27 and Tat PTD was delivered into normal human neuroblastoma SH-SY5Y cells and into SH-SY5Y cells containing hyperphosphorylated tau induced by okadaic acid treatment and obtained protective effect on cell death. However, drugs to treat neurodegenerative diseases must be capable of penetrating the blood-brain barrier (BBB) to be effectively delivered.[32] However, greater than 98 % of all potential CNS drugs cannot cross the BBB.[33] Therefore, we anticipate that the uptake of Tat-Hsp27 into the brain will readily occur when nasally administered and will protect against cell death caused by hyperphosphorylated tau, which is one of the primary causes of AD.[33, 34] Our results suggest that Tat-Hsp27 has a protective effect against hyperphosphorylated tau and could represent a valuable protein therapeutic for AD.

6. References

1. Selkoe DJ., Alzheimer's disease is a synaptic failure. *Science* **2002** *298*:789–791.

2. Kosik KS, Shimura H., Phosphorylated tau and the neurodegenerative foldopathies. *Biochim Biophys Acta* **2005** *1739*:298–310.

3. Medeiros R, Baglietto-Vargas D, LaFerla FM., The role of tau in Alzheimer's disease and related disorders. *CNS Neurosci Ther* **2010** *17*:514–524.

4. Santa-Maria I, Varghese M, Ksie_zak-Reding H, Dzhun A, Wang J, Pasinetti GM., Paired helical filaments from Alzheimer disease brain induce intracellular accumulation of tau protein in aggresomes. *J Biol Chem* **2012** *287*:20522–20533.

5. Crimins JL, Pooler A, Polydoro M, Luebke JI, Spires-Jones TL., The intersection of amyloid beta and tau in glutamatergic synaptic dysfunction and collapse in Alzheimer's disease. *Ageing Res Rev* **2013** *12*:757–763.

6. Chabrier MA, Cheng D, Castello NA, Green KN, LaFerla FM., Synergistic effects of amyloid-beta and wild-type human tau on dendritic spine loss in a floxed double transgenic model of Alzheimer's disease. *Neurobiol Dis* **2014** *64*:107–117.

7. Hernandez F, Avila J., Tauopathies. *Cell Mol Life Sci* **2007** *64*:2219–2233.

8. (a) Andorfer C, Kress Y, Espinoza M, Silva RD, Tucker KL, Barde Y-A, Duff K, Davies P., Hyperphosphorylation and aggregation of tau in mice expressing normal human tau isoforms. *J Neurochem* **2003** *86*:582–590; (b) Citron M., Alzheimer's disease: strategies for disease modification. *Nat Rev Drug Discov* **2010** *9*:387–398.

9. (a) Go¨tz J, Chen F, Dorpe JV, Nitsch RM., Formation of neurofibrillary tangles in P301L tau transgenic mice induced by A b42 fibrils. *Science* **2001** *293*:1491–1495; (b) Denk F, Wade-Martins R., Knock-out and transgenic mousemodels of tauopathies. *Neurobiol Aging* **2009** *30*:1–13; (c) Baglietto-

Vargas D, Kitazawa M, Le EJ, Estrada-Hernandez T,Rodriguez-Ortiz CJ, Medeiros R, Green K, LaFerla FM., Endogenousmurine tau promotes neurofibrillary tangles in 3xTg-AD mice without affecting cognition. *Neurobiol Dis* **2014** *62*:407–415.

10. Bue´e L, Bussie´re T, Bue´e-Scherrer VR, Delacourte A, Hof PR., Tau protein isoforms, phosphorylation and role in neurodegenerative disorders. *Brain Res Rev* **2000** *33*:95–130.

11. Saidi Laiq-Jan, Polydoro Manuela, Kay Kevin R, Sanchez Laura, Mandelkow Eva-Maria, Hyman Bradley T, Spires-Jones Tara L., Carboxy terminus heat shock protein 70 interacting protein reduces tau-associated degenerative changes. *J Alzheimers Dis* **2015** *44*:937–947.

12. Salminen A, Ojala J, Kaarniranta K, Hiltunen M, Soininen H., Hsp90 regulates tau pathology through co-chaperone complexes in Alzheimer's disease. *Prog Neurobiol* **2011** *93*:99–110.

13. Carrettiro Daniel C, Hernandez Israel, Neveu Pierre, Papagiannakopoulos. Thales, Kosik Kenneth S., The cochaperone BAG2 sweeps paired helical filament-insoluble tau form the microtuble. *J Neurosci* **2009** *29*(7):2151–2161.

14. Patil Sachin P, Tran Nhung, Geekiyanage Hirosha, Liu Li, Chan Christina., Cucumin-induced upregulation of the abti-tau cochaperone BAG2 in primary rat cortical neurons. *Neurosci Lett* **2013** *554*:121–125.

15. (a) Shimura H, Miura-Shimura Y, Kosik KS., Binding of tau to heat shock protein 27 leads to decreased concentration of hyperphosphorylated tau and enhanced cell survival. *J Biol Chem* **2004** *279*:17957–17962; (b) Shimura H, Schwartz D, Gygi SP, Kosik KS., CHIP-Hsc70 complex ubiquitinates phosphorylated tau and enhances cell survival. *J Biol Chem* **2004** *279*:4869–4876.

16. Read DE, Gorman AM., Heat shock protein 27 in neuronal survival and neurite outgrowth. *Biochem Biophys Res Commun* **2009** *382*:6–8.

17. Kwon JH, Kim J-B, Lee K-H, Kang S-M, Chung N, Jang Y, Chung JH.,

Protective effect of heat shock protein 27 using protein transduction domain-mediated delivery on ischemia/reperfusion heart injury. *Biochem Biophys Rea Commun* **2007** *363*:399–404.

18. Stetler RA, Gan Y, Zhang W, Liou AK, Gao Y, Cao G, Chen J., Heat shock proteins: cellular and molecular mechanisms in the central nervous system. *Prog Neurobiol* **2010** *92*:184–211.

19. Arrigo A-P., Human small heat shock proteins: protein interactomes of homo- and hetero-oligomeric complexes: an update. *FEBS Lett* **2013** *587*:1959–1969.

20. Song IS, Kang S-S, Kim E-S, Park H-M, Choi CY, Tchah H, Kim JY., Heat shock protein 27 phosphorylation is involved inepithelial cell apoptosis as well as epithelial migration during corneal epithelial wound healing. *Exp Eye Res* **2014** *118*:36–41.

21. Becker-Hapak M, McAllister SS, Dowdy SF., TAT-mediated protein transduction into mammalian cells. *Methods* **2001** *24*:247–256.

22. Green I, Christison R, Voyce CJ, Bundell KR, Lindsay MA., Protein transduction domains: are they delivering? *Trends Pharmacol Sci* **2003** *24*:213–215.

23. Zhang Z, Simpkins JW., Okadaic acid induces tau phosphorylation in SH-SY5Y cells in an estrogen-preventable manner. *Brain Res* **2010** *1345*:176–181.

24. Jakob U, Gaestel M, Engel K, Buchner J., Small heat shock proteins are molecular chaperones. *J Biol Chem* **1993** *268*:1517–1520.

25. Concannon CG, Gorman AM, Samali A., On the role of Hsp27 in regulating apoptosis. *Apoptosis* **2003** *8*:61–70.

26. Goedert M, Jakes R, Vanmechelen E., Monoclonal antibodyAT8 recognises tau protein phosphorylated at both serine 202 and threonine 205. *Neurosci Lett* **1995** *189*:167–170.

27. Kamat PK, Rai S, Nath C., Okadaic acid induced neurotoxicity: an emerging tool to study Alzheimer's disease pathology. *Neurotoxicology* **2013**

37:163–172.

28. Wischik CM, Harrington CR, Storey JMD., Tau-aggregation inhibitor therapy for Alzheimer's disease. *Biochem Pharmacol* **2014** *88*:529–539.

29. Ahn J, Kim H, Park J-S., Hsp27 reduces phosphorylated tau and prevents cell death in the human neuroblastoma cell line SHSY5Y. *Bull Korean Chem Soc* **2013** *34*:1503–1507.

30. Wadia JS, Dowdy SF., Transmembrane delivery of protein and peptide drugs by TAT-mediated transduction in the treatment of cancer. *Adv Drug Deliv Rev* **2005** *57*:579–596.

31. Rogers M-L, Rush RA., Non-viral gene therapy for neurological diseases, with an emphasis on targeted gene delivery. *J Controll Release* **2012** *157*:183–189.

32. Ozsoy Y, Gungor S, Cevher E., Nasal delivery of high molecular weight drugs. *Molecules* **2009** *14*:3754–3779.

33. Brasnjevic I, Steinbusch HWM, Schmitz C, Martinez-Martinez P., Delivery of peptide and protein drugs over the blood–brain barrier. *Prog Neurobiol* **2009** *87*:212–251.

34. Schwarze SR, Ho A, Vocero-Akbani A, Dowdy SF., In vivo protein transduction: delivery of a biologically active protein into the mouse. *Science* **1999** *285*:1569–1572.

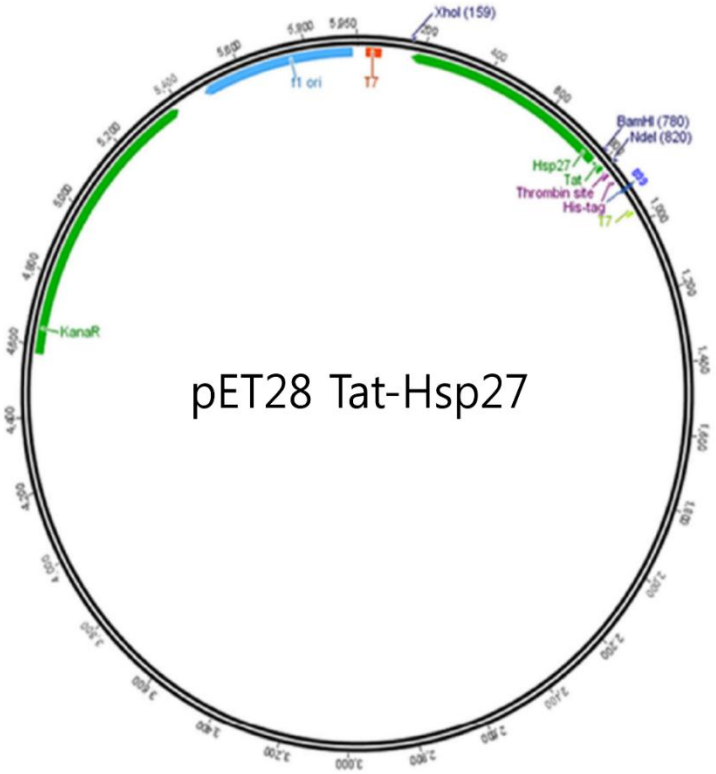

Figure 1. pET28 vector containing hexahistidine (6X His) and Tat protein transduction domain and Hsp27 cDNA

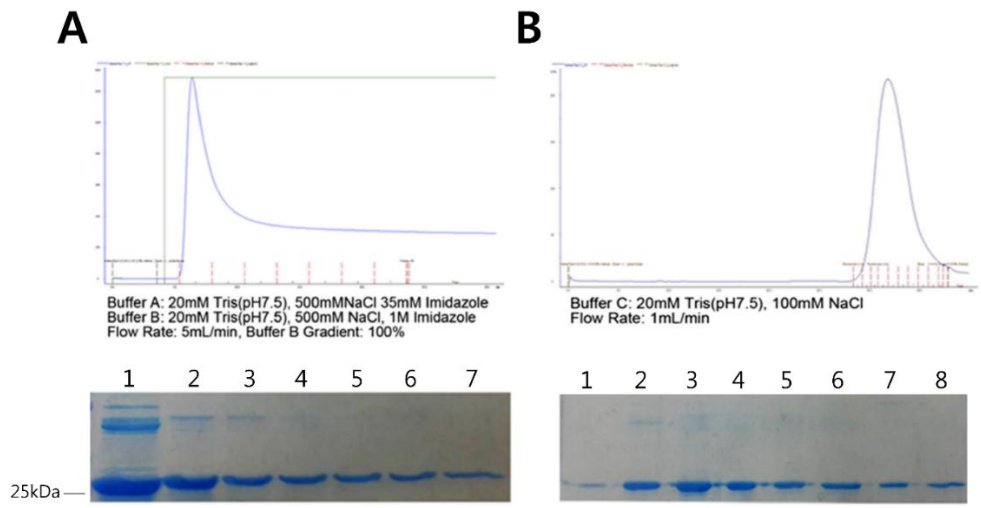

Figure 2. Tat-Hsp27 protein purification. A) His-tagged Tat-Hsp27 was eluted from the affinity chromatography column using isocratic elution buffer (20 mM Tris-HCl, pH 7.5, 500 mM NaCl, and 1 M imidazole). B) His-tagged Tat-Hsp27 was further purified using size exclusion chromatography (20 mM Tris-HCl, pH 7.5, and 100 mM NaCl) and eluted as a single peak. Fractions were analyzed using SDS-PAGE after each purification step.

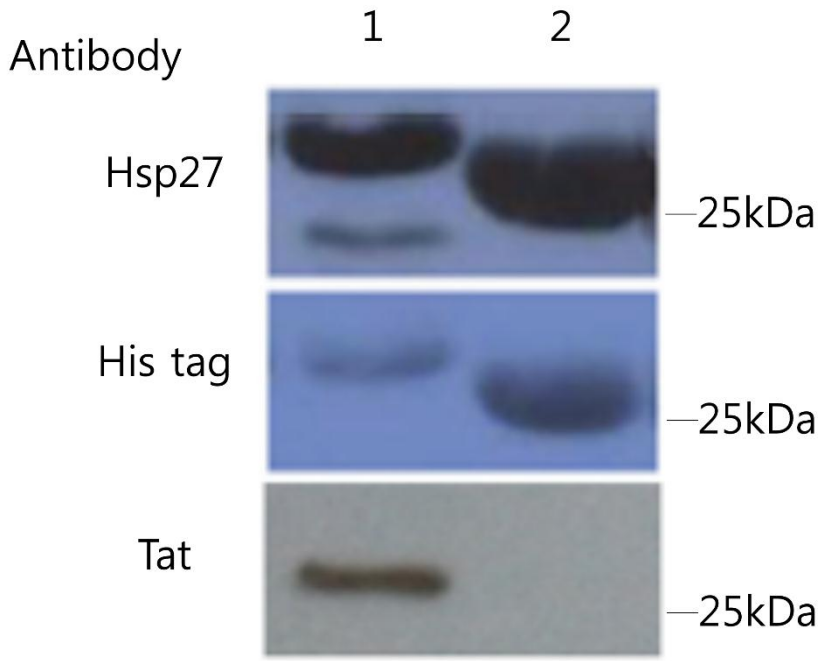

Figure 3. Western blot analysis of purified Histagged Tat-Hsp27 using anti-His tag, anti-Hsp27, and anti-Tat antibodies.

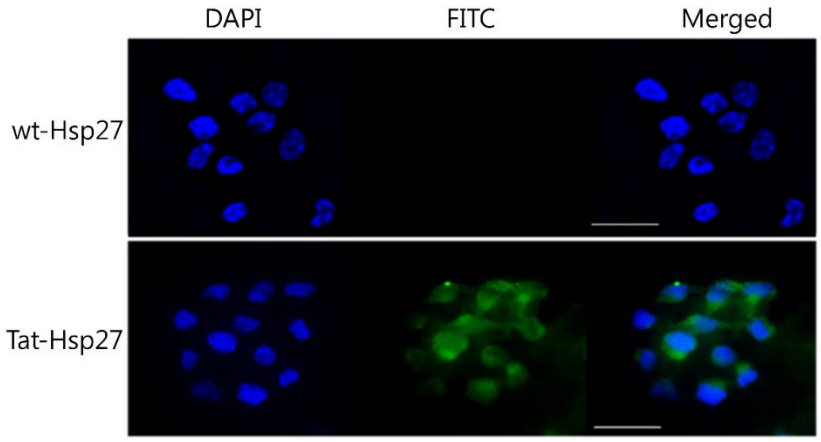

Figure 4. Immunocytochemistry. FITC conjugated wt-Hsp27 or Tat-Hsp27 was delivered into cells and analyzed 2 h later. Image restoration microscopy indicates that Tat-Hsp27 was rapidly and efficiently delivered, in contrast to wt-Hsp27. Scale bar 30 μm.

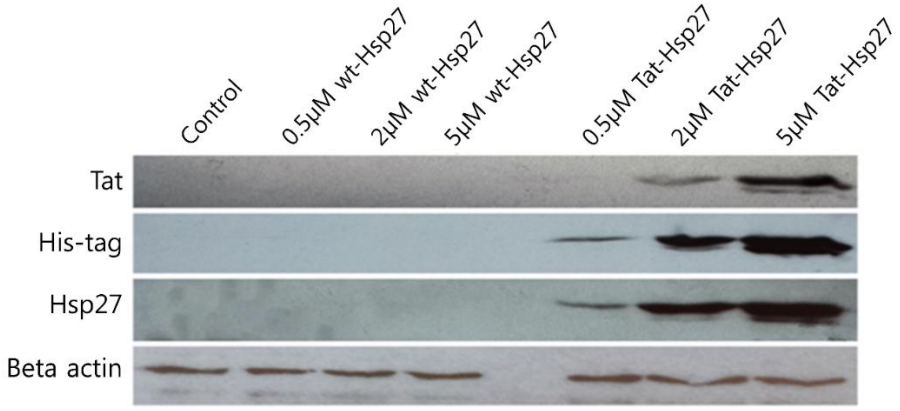

Figure 5. Protein from cell lysates in western blot. Protein from cell lysates of SH-SY5Y cells treated with wt-Hsp27 or Tat-Hsp27 was analyzed using Western blot analysis. The protein expression was normalized to actin.

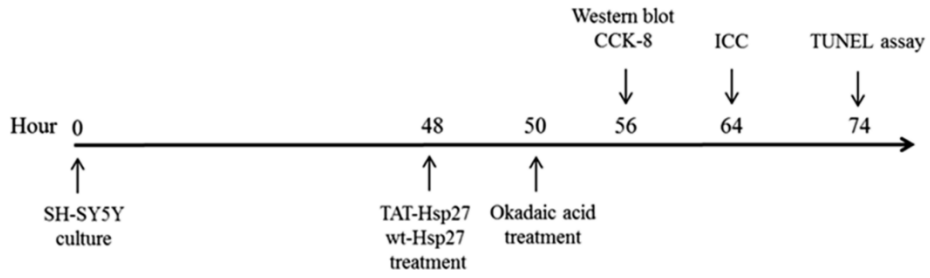

Figure 6. Experimental design for Tat-Hsp27 treatment in SH-SY5Y cells.

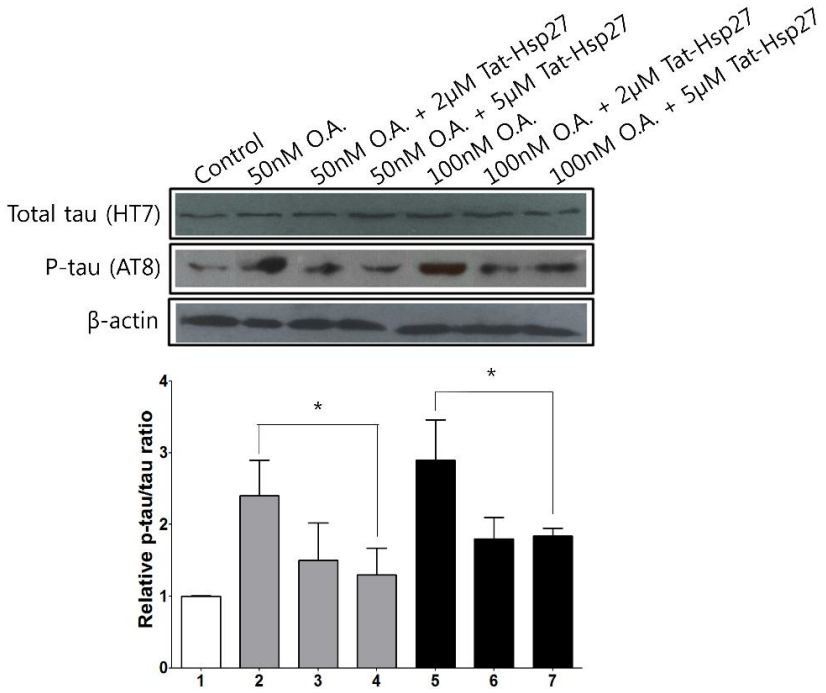

Figure 7. Effect of Tat-Hsp27 on tau hyperphosphorylation. Western blot analysis of total tau (HT 7) and p-tau (AT 8), with beta-actin as a loading control. *p < 0.05 compared with the control. **p < 0.01 compared with okadaic acid alone. Values indicate mean ± SD (Anova, Tukey's HSD test, n = 3 per group).

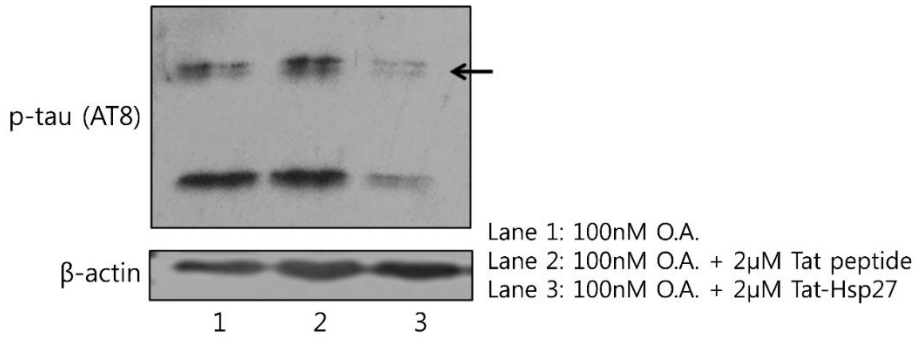

Figure 8. Effect of Tat peptide and Tat-Hsp27 on tau hyperphosphorylation. Western blot analysis of p-tau (AT 8).

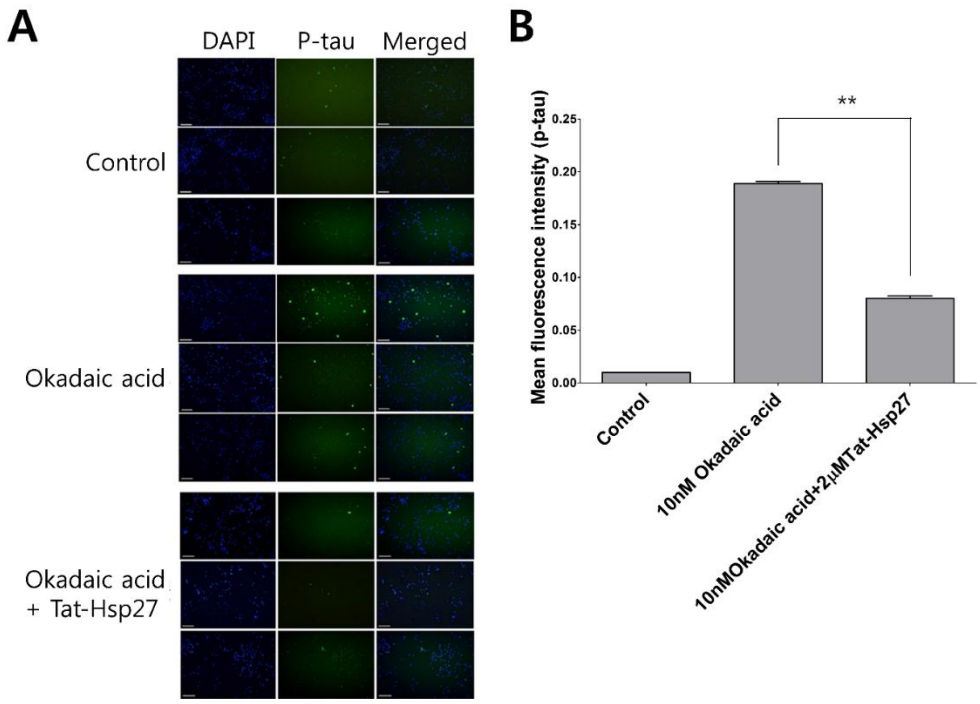

Figure 9. Representative immunofluorescence images. A) SH-SY5Y cells were treated with 2 μM Tat-Hsp27 (2 h) followed by 10 nM okadaic acid (14 h). All cells were fixed and stained with primary antibodies against p-tau (AT 8) and the corresponding fluorescent secondary antibody. Green (FITC) indicates phosphorylated tau. Scale bar 100 μm. B) Quantitation of the immunofluorescence intensity demonstrated that phosphorylated tau by Okadaic acid was decreased by treatment with Tat-Hsp27. Values indicate mean ± SD (Anova, Tukey's HSD test, n = 3 per group). *$p < 0.05$ compared with okadaic acid alone.

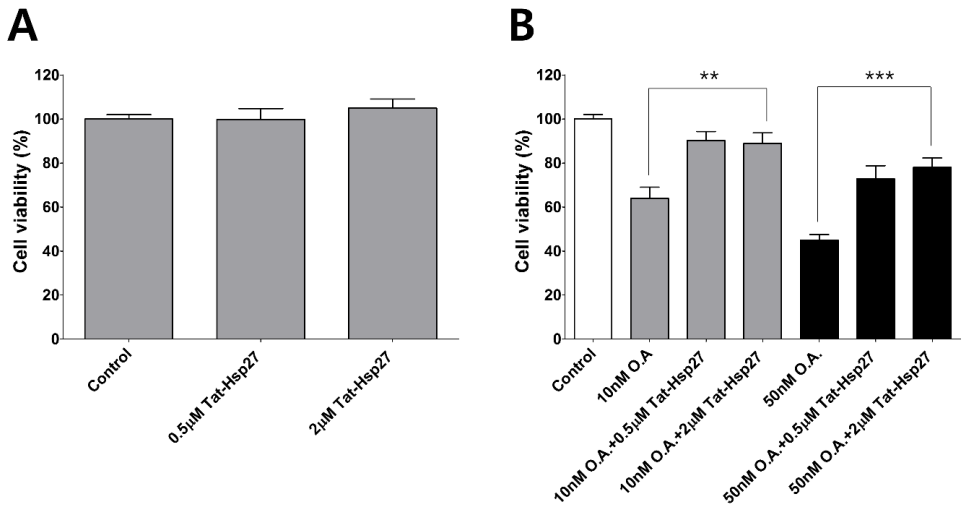

Figure 10. Cytotoxicity assay using the Cell Counting Kit-8. SH-SY5Y cells were transduced with 0.5 or 2 μM Tat-Hsp27 alone A) or prior to treatment with 10 and 50 nM okadaic acid. B) The transduction of Tat-Hsp27 alone does not affect the cell viability. *$p < 0.05$ compared with the control. **$p < 0.01$ compared with okadaic acid alone. Values indicate mean ± SD (Anova, Tukey's HSD test, n = 7 per group).

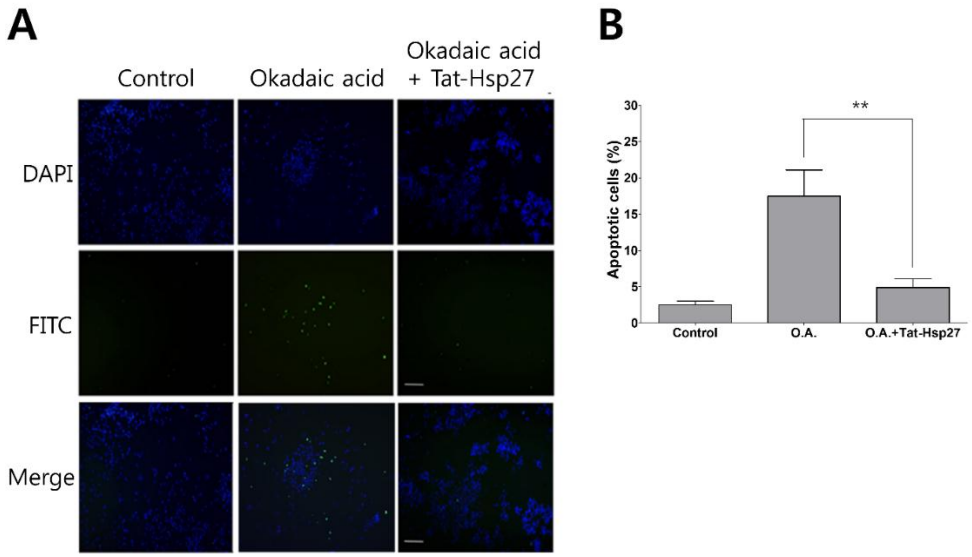

Figure 11. Tat-Hsp27 inhibits apoptotic cell death induced by okadaic acid. The TUNEL assay was performed to determine the extent of programmed cell death. SH-SY5Y cells were treated with 10 nM okadaic acid alone or following pretreatment with 2 μM Tat-Hsp27. A) Representative images of the TUNEL assay. Scale bar 100 μm. B) Quantitation of the percentage of TUNEL-positive cells indicated that apoptosis induced by okadaic acid was decreased in cells pretreated with Tat-Hsp27. Values indicate mean ± SD (Anova, Tukey's HSD test, n = 3 per group). *$p < 0.05$.

Part B. Development of New Type of Cell-Penetrating Peptide Fusion Protein and Application for Transcriptional Control

Rapid Intracellular Protein Transport at Nanomolar Concentrations by Multimeric Amphipathic α-Helical Sequences

1. Abstract

An amphipathic leucine (L) and lysine (K)-rich α-helical peptide was multimerized based on helix-loop-helix structures to maximize the penetrating activities. The multimeric LK-based cell penetrating peptides (LK-CPPs) could penetrate cells as protein-fused forms at 100–1,000 fold lower concentrations than Tat-proteins. The enhanced penetrating activity was increased through multimerization by degrees up to the tetramer level. The multimeric LK-CPPs showed rapid cell penetration through macropinocytosis at low nanomolar concentrations, unlike the monomeric LK, which had slower penetrating kinetics at much higher concentrations. The heparan sulfate proteoglycan (HSPG) receptors were highly involved in the rapid internalization of multimeric LK-CPPs. As a proof-of-concept of biomedical applications, we delivered an adipogenic transcription factor, PPAR-γ2, into pre-adipocytes, and induced highly enhanced expression of adipogenic genes at nanomolar concentrations. The multimeric CPPs can be a useful platform for the intracellular delivery of biomacromolecular reagents that have difficulty with penetration in order to control biological reactions in cells at feasible concentrations for biomedical purposes.

2. Introduction

Biomacromolecules such DNA, RNA, and proteins are considered to be potential biomedical reagents for the control of selective biological reactions.[1] Since most biomacromolecules have difficulty penetrating cells through their plasma membranes, various methodologies based on viral and non-viral delivery systems have been applied for the intracellular delivery of biomacromolecules.[2] Although viral systems show outstanding delivery efficiency, they often face critical safety issues in clinical trials.[2a, 3] On the other hand, non-viral systems exhibit rather limited delivery efficiency, but are relatively free from safety issues.[2a, 4] Thousands of chemical and biological strategies have been challenged to overcome the biocompatibility and delivery efficiency barriers of conventional techniques.[5]

Existing between the chemical and biological strategies, cell penetrating peptides (CPPs) and protein transduction domains (PTDs) are highlighted as powerful tools for facilitating the intracellular delivery of biomacromolecules.[6] After the first discovery of the Tat sequence from a HIV protein[7], a number of CPPs have been applied to the intracellular translocation of hard-to-penetrate biomolecules.[8] Chemically synthesized CPPs are covalently or non-covalently hybridized to biomedical reagents to enhance cell penetration and drug efficacy.[9] Moreover, CPPs are highly desirable for intracellular protein delivery because CPP sequences can be readily inserted into protein sequences using genetic recombination techniques.[10] Various proteins have been delivered into the cell interiors in CPP-fused forms to correct disordered biochemical reactions[11], induce apoptosis[12], or control cell lineages[13] for corresponding biomedical objectives.

CPPs have many advantages over other delivery techniques. They are capable of simple and systematic synthesis by both chemical and biological methods,

high biocompatibility due to naturally-originated amino acid-based structures, efficient tissue penetration, and may be combined in a versatile fashion with both viral and non-viral delivery systems. However, one of the greatest weaknesses impeding the broad biomedical application of CPPs is the penetration concentration, *i.e.* the extracellular concentration threshold at which showing significant penetration of peptides. Most CPPs or CPP-conjugated cargos are internalized into cells only at micromolar concentrations.[14] The micromolar penetrating concentrations may be acceptable for the delivery of small molecules, but it is expensive and impractical to administer micromolar doses of biomacromolecules. We believe that it is essential to discover or develop new CPPs that are able to deliver macromolecular cargo into cells at clinically feasible concentrations for future practical CPP-based therapeutic applications.

The CPPs that have previously been reported are generally categorized into two structural types, multi-positively charged sequences and amphipathic cationic sequences. In this study, we found that the multimerization of amphipathic α-helical peptide sequences could greatly reduce the penetrating concentration and accelerate the penetration rate of the CPPs. Particularly in case of over tetrameric sequences, the multimeric peptides showed rapid protein internalization within 30 min through direct penetration or unique endocytic mechanisms at nanomolar concentrations. Shorter sequences or conventional CPPs showed a much slower internalization through different endocytic mechanisms even at far higher micromolar concentrations. As the first step of biomedical application, we were able to induce adipocyte differentiation effectively by delivering the multimeric CPP-fused form (tetrameric form) of a key transcription factor called peroxisome proliferator-activated receptor gamma 2 (PPAR-γ2) at nanomolar concentrations.

3. Materials and Methods

3.1. Cell lines and cell culture

HeLa (human cervix epithelial carcinoma), HEK 293T (human embryotic kidney), MDA-MB-231 (human breast cancer) cells were purchased from the American Type Culture Collection (ATCC) and maintained in high glucose Dulbecco's modified Eagle's medium containing 10% (v/v) fetal bovine serum (FBS) (Wellgene) at 37 °C in the presence of 5% CO_2. CHO K1 (Chinese hamster ovary) cells were purchased from Korean Cell Line Bank (KCLB) and cultured in Ham's F12 medium containing 10% fetal bovine serum (FBS) at 37 °C in the presence of 5% CO_2. HEK 293s GnTI- (human embryotic kidney) cells (ATCC) were cultured under standard condition in Dulbecco's modified Eagle's medium and F12 ratio 1:1 medium containing 10% fetal bovine serum (FBS) at 37 °C in the presence of 5% CO_2. 3T3-L1 (*mus musculus* embryo fibroblast) (KCLB) cells were maintained in Dulbecco's modified Eagle's medium containing 10% bovine calf serum (BCS) (Wellgene) and incubated at 37 °C in the presence of 5% CO_2.

3.2. Peptide Synthesis

Solid Phase Peptide Synthesis: For Fmoc deprotection, the resins were placed in a microwave vessel and irradiated for 2 min (ramping time for 1 min) at 5 W power. For the coupling step, the resins were microwave irradiated for 5 min (ramping time for 2 min) at 5 W power. The temperature was set at 35 °C for both steps.

Dimerization of Peptides: Dimeric bundle peptides were prepared by air oxidation as previously described.[15a, 35] Briefly, cysteine-containing peptide monomer was dissolved in 0.1 M deaerated ammonium bicarbonate to give a final concentration of 1 mg/mL and the mixture was incubated to stand open to atmosphere until the reaction was complete. Parallel and antiparallel dimers

were obtained and shown to be separated by HPLC using a C18 column (Zorbax C18, 3.5 mm, 4.6 × 150 mm) as the stationary phase and buffer A (water with 0.1%, v/v TFA) and buffer B (acetonitrile with 0.1%, v/v TFA) as the mobile phase. Parallel dimers are major products (antiparallel dimers were obtained less than 5% judged by HPLC traces) and found to be relatively nonpolar than antiparallel minor dimers as described previously (22). Dimeric peptides were confirmed by using MALDI-TOF and purified by a preparative HPLC.

Fluorescence Labeled Peptides: The dye 5-TAMRA (Merck Millipore) was used to lead fluorescently labeled peptides. The fluorescent dye was coupled at the *N*-terminus of each peptide using 2-(6-choloro-1-H benzotriazole-1-yl)-1,1,3,3-tetramethylaminum hexafluorophosphate (HCTU) activation. Briefly, 5-TAMRA (2 eq, relative amount to Fmoc deprotected N-terminus amine) was dissolved in anhydrous dimethylformamide (DMF) to a final concentration of 0.1−0.5 M and activated with HCTU (2 equiv), 1-hydroxybenzotriazole (HOBt, 2 equiv), and diisopropylethylamine (4 equiv). The activated 5-TAMRA solution was added to the Fmoc deprotected resin and stirred for 2 h at room temperature. When the reaction was complete, peptides were cleaved from resins followed by the normal procedure. For dimer peptides, 5-TAMRA was labeled on only one strand (Figure 1).

3.3. Construction of the expression vectors

We designed a bacterial expression vectors containing hexahistidine leader sequence. A gene encoding enhanced green fluorescence protein (eGFP) in the C2-eGFP vector was amplified by PCR using the C2-eGFP as a template and oligonucleotide primers containing *BamHI* and *XhoI* (New England Biolabs) restriction sites. The pET28b vector and the amplified eGFP gene were digested with *BamHI* and *XhoI* and ligated (New England Biolabs) to make pET28b-eGFP as a negative control. Tat encoded gene (Cosmo Genetech) was amplified by PCR using primers containing *NdeI* and *BamHI*. Both the vector and PCR

fragment were digested by *NdeI* and *BamHI* restriction enzymes and ligated to make pET28b-Tat-eGFP vector as a positive control. For LK-1-eGFP, a gene encoded LK-1 in the pUC vector was produced by gene synthesis (Cosmo Genetech). The LK-1 gene was amplified using PCR and cloned into a pET28 vector, and the gene encoding eGFP was inserted later. For LK-2-eGFP, a gene encoded LK-2 in the pUC vector was produced by gene synthesis, cloned into pET28b-eGFP. For LK-3-eGFP, the PCR product of LK-2 gene was inserted into pET28b-LK-1-eGFP. For LK-4-eGFP, the PCR product of LK-2 gene was ligated with pET28b-LK-2-eGFP. For LK-5- and LK-6-eGFPs, the LK-4 fragment without restriction sites was synthesized by gene synthesis. Later, the LK-4 sequence was inserted into LK-1-eGFP and LK-2-eGFP to produce LK-5-eGFP and LK-6-eGFP, respectively. For PPAR-γ2 vectors, we purchased pBABE puro PPAR γ2 vector from addgene. pET28b vector was digested by *NdeI* and *XhoI* and ligated with the PPAR-γ2 PCR fragment to construct pET28b-PPAR-γ2 vector. pET28b-LK-4-PPAR-γ2 vector was generated by ligation between the PCR products of pET28b-LK-4-eGFP and PPAR-γ2 with *SacI* and *XhoI* primers. Each PCR primer sequence was summarized in Table 1.

3.4. Purification of recombinant proteins

All recombination proteins were expressed using bacterial systems. *Escherichia coli Rosetta* (DE3) pLysS (Novagen) were transformed with plasmids encoding recombinant proteins and incubated in 10 mL of LB broth containing kanamycin and chloramphenicol for 16 h at 37 °C. Then, the cultures were transferred into 1 L of fresh LB medium and incubated at 37°C for further 2-3 h until OD_{600} reached 0.4-0.6. Isopropyl-β-thiogalactopyranoside (1 mM) was added to the media. The cells were incubated overnight at 16 °C with shaking at 190 rpm, subsequently. The cells were then harvested by centrifugation at 6000 rpm for 10 min at 4 °C and re-suspended in a lysis buffer (20 mM Tris, 500 mM NaCl, 35 mM imidazole, 0.05% Triton X-100, pH 7.0).

After the suspension was sonicated by the ultrasonic processor (Sonic & Materials, Inc), the supernatant was obtained by centrifugation at 13000 rpm for 20 min at 4 °C. The supernatant was filtered through 0.22 μm syringe filters, and the 6-His-tagged proteins were purified via Ni-NTA affinity chromatography (GE Healthcare) and desalted with a solution containing 20 mM Tris, 200 mM KCl, 1 mM DTT and 10% glycerol through a 30K Amicon centrifuge filter (Milipore). The protein solution could be further purified by a Superdex 200 16/60 (GE Healthcare) size column with an eluent containing 20 mM Tris and 400 mM NaCl (pH7.5). Protein concentrations were measured using the Quick Bradford assay (Bio-Rad). Purified proteins were stored in a solution containing 20 mM Tris, 200 mM KCl, 1 mM DTT and 10% glycerol.

3.5. Measurement of cell penetration activities

Cells (8×10^4 cells/well) were seeded in 24-well plates and incubated in DMEM containing 10% FBS overnight. Recombinant eGFP proteins were added to the cells at various concentrations and further incubated for 12 h. For the experiment of penetrating kinetics, the incubation time was varied. For the endocytosis inhibition assay, cells were pre-treated with endocytosis-inhibiting conditions before the protein treatment: 4 °C incubation for 1 h or treatment of 10 mM sodium azide (NaN_3), 50 μM amiloride or 100 μM wortmannin for 3 h. The cells were washed thoroughly with DPBS (×3) and incubated with trypsin-EDTA (0.25%) for 10 min at 37 °C to digest the proteins bound to the cell surface. Detached cells were harvested and centrifuged at 13000 rpm for 10 min and suspended in DPBS containing 2% FBS. The FACS analysis was performed on FACS Calibur (Becton Dickinson, U.S.A.). A total of 1×10^4 cells were assessed for each sample and dead cells were excluded from the analysis.

3.6. Confocal laser fluorescence microscopy

Cells (1.5×10^4 cells/well) were seeded on confocal dish (SPL) and incubated

at 37 °C, 5% CO_2. After 24 h, the cells were treated with recombinant eGFP proteins in fresh complete medium at 37 °C at various concentrations. A Hoechst 33342 dye solution (Thermo Fisher Scientific) was added to the cells at a final concentration of 1 μg/mL, and the cells were incubated for 10 min. The cells were washed thoroughly with DPBS (×3) to remove proteins bound to the cell surface. After the additon of fresh complete media, images were acquired using an LSM 510 laser scanning confocal microscope (Carl Zeiss, Oberkochen, Germany) with a 400× objective.

3.7. LDH assay

HeLa cells (1×10^4 cells/well) were seeded in 96-well plates and incubated for 24 h. The media was exchanged and cells were treated with proteins for further 24 h. The LDH assay was performed with the Pierce LDH Cytotoxicity Assay Kit (Thermo Scientific) following manufacturer's protocols. The absorbance was measured using the multi-functional microplate reader Infinite 200PRO (TECAN).

3.8. Heparin interaction assay

Heparin interaction assay was performed with the biolayer interferometer, the BLItz System (Pall ForteBio). The surface of AR2G tip (Octet biosensors) was activated in deionized water for 30 s and then exposed to a solution of branched polyethylenimine (1 mM in PBS, Mw = 25,000, Sigma-Aldrich) for 250 s for the formation of positively charged surface. Then, a heparin sodium salt solution (100 μM in PBS, Millipore 375095) was allowed to flow on the surface for another 250 s for the immobilization of heparin through electrostatic interaction. The multi-layered surface was washed with PBS for 60 s. A protein sample was associated with the sensor for 100 s by the flow of protein solutions (2.5 μM in PBS) and dissociated for 100 s by washing the surface with PBS.

3.9. XylT-I knockdown assay

HeLa cells (5×10^4 cells/well) were seeded in 24-well plates and incubated for 24 h. The cells were transfected with XylT-I siRNA (40 pmol, Santa Cruz) using Lipofectamine 2000 (1 μL, Invitrogen) following the following manufacturer's protocols. After the treatment of the XylT-I siRNA complex for 48 h, LK-4-eGFP protein was treated for 1 h at various concentrations. Control siRNA (Santa Cruz) was used as a control. The knockdown assay in HEK293T and HEK293s GnTi- cells was performed in a similar manner except for the initial cell density (1.5×10^4 cells/well).

3.10. Cell viability assay

A cytotoxicity assay was performed using the cell counting kit-8 (Dojindo, Korea). *HeLa* cells (5×10^3 cells/well) were seeded in 96-well plates and incubated for 24 h. Then, growth media was replaced with fresh culture media (100 μL/well) containing 1% FBS, and the cells were treated with samples with various concentrations of proteins for 24 h, 48 h and 72 h. Following the incubation, 10 μL of CCK-8 solution was added, and the cells were incubated at 37 °C for 1 h. The absorbance at 450 nm was measured using a microplate reader (Molecular Device Co., Menlo Park, CA).

3.11. Adipocyte differentiation

3T3-L1 cells (2×10^4 cells/well) were grown in high glucose DMEM supplemented 10% fatal bovine serum (FBS) in 48-well plate. At confluence (Day 0), the cells were first treated with recombinant proteins. Protein was treated every single day from Day 0 to Day 8. The cells were washed once in DPBS (Wellgene) and fixed with 4% paraformaldehyde in DPBS for 20 min, followed by Oil O Red staining method described previously.[36] DIC images were obtained using an inverted microscope (**Zeiss Axio Observer Z1)**. For RT-PCR, total RNA were isolated from the cells using a NucleoSpin RNA kit (MN). 1 μg of RNA was reverse transcribed using the QuantiTech reverse

transcription kit (Quiagen). SYBR green reactions using KAPA SYBR fast qPCR kit (Biosystems) were performed with BioRad CFX connect real time PCR equipment (BioRad). Relative expression of mRNA was determined after normalization to total RNA amount. The primers were summarized in Table 2.

3.12. Statistical analysis

The data were analyzed using two-tailed Student's t-tests. P values < 0.05 were considered as significant differences. Differences are presented on graphs as *, **, ***, and ****, which indicate $0.01 \leq p < 0.05$, $0.001 \leq p < 0.01$, $0.0001 \leq p < 0.001$ and $p < 0.0001$, respectively. The indication of 'ns' means that there was no significant difference.

4. Results and Discussion

4.1. Nanomolar cell penetration of LK multimers

We have recently discovered that the penetrating concentration of a 16-meric amphipathic α-helical peptide (LKKLCKLLKKLCKLAG; LK-peptide) could be greatly reduced by dimerization between two LK-peptide molecules through the oxidative formation of two disulfide bonds.[15] Remarkably, the dimeric peptide with an antiparallel structure as the major form can penetrate cells and inhibit the RNA transcription of HIV genes at nanomolar concentrations over 100-fold lower than to the penetrating concentrations of other conventional CPPs such as Tat or oligoarginines.

In nature, α-helical bundles such as helix-loop-helix (HLH) and helix-turn-helix motifs are frequently observed in coiled coil proteins.[16] The antiparallel LK-dimer has a close resemblance to that of natural HLH motifs with the exception of the fact that the monomeric units in the dimer are linked via disulfide bonds. We expected that a HLH motif with a similar sequence could mimic the antiparallel LK-dimer for high cell penetrating activity. The HLH motif can be linearly synthesized through chemical methods such as solid-phase peptide synthesis (SPPS) with higher yields than the disulfide-based LK-dimer which requires an additional dimerization step. Furthermore, the HLH motif can also be prepared and readily fused with cargo proteins through genetic recombination. Therefore, starting from LKKLLKLLKKLLKLAG (LK-1), which replaced the cysteines (C) of the LK peptide with leucines (L) for the prevention of premature and irregular disulfide formation during protein translation, we prepared LK-2 with a linearly duplicated sequence of the LK-1 and glycine-glycine (GG) dipeptides in the middle of the sequence (Figure 2A). We intended for the GG sequence to be able to form a flexible turn (or loop) between two α-helices for the antiparallel HLH structure.[17] The α-helical propensity of LK-2 was significantly enhanced in comparison to LK-1 as

shown in the Circular Dichroism (CD) spectra (Figure 2B). Especially, LK-2 showed an approximately an α-helical content of 85% in a membrane-mimic condition. The α-helical structure of LK-1 could be stabilized by the linear duplication of the sequences probably due to the helix-helix interactions.

The cell penetrating activity of LK-2 was evaluated in a human cervical cancer cell line (HeLa) through fluorescence-activated cell sorting (FACS). The disulfide-based LK-dimer and Tat sequence were used as references. The cell penetration activities of the fluorescence-labelled peptides were found to increase in the following order: Tat < LK-1 < LK-2 < LK-dimer (Figure 3). The LK-2 displayed slightly lower cell penetrating activity than the LK-dimer; however, there was > 30% penetration at 50 nM, and nearly quantitative penetration at 200 nM. On the other hand, Tat showed only 1% cell penetration even at 1 μM. Clearly, the linear duplicate of the LK peptide that mimics the LK-dimer has much higher cell penetrating activity than conventional CPPs.

We further investigated the effect of the multimerization of the LK sequence. The notations LK-3, LK-4, LK-5, and LK-6 were used for the trimeric, tetrameric, pentameric and hexameric sequences (Table 3) of the LK-1 peptide, respectively, as represented in Figure 4A. Since it is difficult to synthesize peptides with over 50 amino acids through chemical methods, fused proteins with each sequence at the *N*-terminus of a cargo protein were instead prepared by genetic recombination. The linker peptide sequences between the LK monomers in multimeric sequences were somewhat varied due to limit of recombinable sequences in the plasmid where highly repeated sequences could be inserted in the genes for the LK multimers. eGFP was used as a model protein to compare the cell penetrating activities of the multimeric sequences through the measurement of fluorescence. CPP-fusion proteins including Tat-eGFP as a positive control, were successfully prepared by plasmid transformation into *E.coli* and purified by affinity chromatography based on *N*-terminal His-tags (Figure 4B).

The cell penetrating activities of CPP-fused eGFPs were compared in two cell lines using sub-micromolar concentrations, at which Tat and oligoarginine showed only limited cell penetration. Figure 4C and D showed the concentration-dependent penetration efficiency on the HeLa (human cervical cancer) and HEK 293T (human embryonic kidney) cells after a 12 h- treatment using CPP-fused eGFPs. The cell penetrating activities of the CPP-fused eGFPs were dramatically increased by the multimerization of the LK sequences on both cell lines. The Tat-eGFP showed almost negligible penetrating efficiency below 1 μM, but the LK-1-eGFP showed penetrating activity with 40% and 80% of cell being fluorescence-positive (+) at 500 nM and 1 μM, respectively. The LK-2-eGFP with a dimerized CPP showed 40% at 200 nM and almost 100% at 500 nM. The LK-3-eGFP showed even higher cell penetrating activity with over 50% at 100 nM. The enhancement of cell penetrating activity through multimerization was almost saturated over tetramerization. LK-4-, LK-5- and LK-6-eGFP all showed over 50% and almost 100% of cells being fluorescence-(+) at 50 nM and 100 nM, respectively. Figure 4E compares the cell penetrating activities of CPP-fused eGFPs at 100 nM, and illustrates the sharp increase of cell penetrating activities at LK-3-eGFP and saturation after LK-4-eGFP. The intracellular green fluorescence of CPP-eGFPs was visualized at 100 nM concentration through confocal laser scanning microscopy (CLSM) (Figure 5). Corresponding to the FACS data, the numbers and intensities of green pixels clearly increased from LK-1-eGFP to LK-6-eGFP. Under the same conditions, only negligible green fluorescence was observed in Tat-eGFP- treated cells. Most CPP-eGFPs were observed in the cytosol, but a small portion of them were localized in the nuclei stained with DAPI (4’,6-diamidino-2-phenylindole), representing co-localized cyan signals from green and blue fluorescence. The multimeric CPP-eGFPs showed almost no cytotoxicity up to 1 μM, which was far over the effective penetrating concentration of 100 nM (Figure 6).

4.2. The cell penetrating mechanism of LK multimers

We examined the outstanding cell penetrating properties of the multimeric CPPs in more detail by comparing the penetrating kinetics of LK-1-eGFP and LK-4-eGFP at various concentrations. LK-1-eGFP only began to penetrate into HeLa cells after 6 h- of incubation at concentrations below 500 nM (Figure 7A). However, at 1 μM and 2.5 μM, the penetration rate of LK-1-eGFP accelerated, and 70% and 98% of cells were fluorescence-(+) after a 30 min- incubation, respectively. On the other hand, the LK-4-eGFP condition had over 60% of cells fluorescence-(+) within 1 h at 100 nM, and the rate increased with the elevation of the concentration (Figure 7B). At 200 nM and 500 nM, LK-4-eGFP penetrated 55% and 100% of cells within 30 min, respectively. On the basis of this result, we believe that the penetrating mechanism of LK-based CPPs may be dependent upon both the multimerization degree and the concentration (Figure 7C).

CPPs are thought to be internalized into cells through both ATP-dependent and ATP-independent mechanisms.[18] Receptor-mediated endocytosis such as clathrin- or caveolae-mediated endocytosis and macropinocytosis, requires ATP for the uptake of CPPs, whereas intracellular entry through direct penetration via fusion and aggregate formation on the membrane proceeds without ATP.[19] Most CPPs penetrate cells using more than one mechanism.[20] HeLa cells were pre-treated with representative internalization inhibiting conditions: wortmannin (a receptor-mediated endocytosis inhibitor), amiloride (a macropinocytosis inhibitor), sodium azide (an ATP synthase inhibitor), and a 4 °C-incubation (energy depletion)[21], and then were further incubated with LK-1-eGFP and LK-4-eGFP at various concentrations for 1 h in order to compare the penetrating efficiency at the early stage. In the case of LK-4-eGFP, the inhibition profile clearly changed according to the concentration (Figure 7D). At 100 nM, LK-4-eGFP showed approximately 50% of cells being

fluorescence-(+) at the 1 h point. Energy depletion inhibited the penetration almost completely implying that the entry mechanism was ATP-dependent. The significant inhibition of the penetrating activity through the sodium azide treatment also supported the concept that the internalization of LK-4-eGFP was ATP-dependent. By comparing the fluorescence in the wortmannin and amiloride treatments, which showed almost no inhibition and 70% inhibition, respectively, we concluded that LK-4-eGFP predominantly utilizes ATP-dependent endocytosis mechanisms at this low concentration, mainly macropinocytosis rather than receptor-mediated endocytosis. The penetrating activity of LK-4-eGFP at 500 nM, however, was almost unaffected by the inhibition conditions. This result supported the thought that LK-4-eGFP rapidly penetrated cells through ATP-independent pathways at 500 nM. A marginal increase in membrane destabilization was observed in the lactate dehydrogenase (LDH) assay at 500 nM, but the destabilization degree was very limited (< 6%) (Figure 8).

As mentioned above, the penetration of LK-1-eGFP was much slower than LK-4-eGFP at concentrations below 1 μM, but was somewhat accelerated at the 1 μM and 2.5 μM concentrations. Even in this high concentration, LK-1-eGFP showed only ATP-dependent penetration that was likely to be both receptor-mediated endocytosis and macropinocytosis, based on the results of complete inhibition at 4 ℃ and the approximately 50–70% inhibition in the sodium azide, wortmannin, and amiloride conditions.

It has often been reported that many cationic CPPs were internalized by the mediation of extracellular glycosaminoglycans such as heparan sulfate proteoglycans (HSPG).[22] We wondered if HSPG would be the key mediator to induce the rapid internalization of multimeric CPPs at nanomolar concentrations. MDA-MB-231 (human breast cancer) cells, which expressed a massive amount of HSPG[23], and CHO-K1 (Chinese hamster ovary) cells that lacked 3-O-sulfotransferase, the key enzyme for the HSPG maturation[24], were

selected to examine the effect of HSPG on the penetration of LK-eGFPs. All types of LK-eGFPs showed increased penetration at nanomolar concentrations in MDA-MB-231 cells (Figure 9A) compared to the results from HeLa and HEK 293T (Figure 4C and D). However, LK-eGFPs showed very limited cellular penetration in CHO-K1 cells in the concentration ranges up to 100 nM and only began to penetrate cells over 200 nM with low efficiency (Figure 9B). Figure 9C compares the fluorescence-(+) cells among MDA-MB-231 and CHO-K1 treated with of LK-4-eGFP at 100 nM and 500 nM after 12 h-incubation. Interestingly, LK-4-eGFP showed a large difference in penetrating activities (100% vs. 0.5%) at 100 nM, but the difference was almost negligible at 500 nM, showing 100% and 97% on the HSPG-rich MDA-MB-231 and the CHO-K1 cells with immatured HSPG, respectively. In addition, the penetration of LK-4-eGFP into CHO-K1 cells only began after 6 h at 200 nM (Figure 9D), unlike the rapid penetration into the HeLa cells, which occurred within 1 h (Figure 7B) at the same concentrations. On the other hand, the rapid internalization of LK-4-eGFP was similarly observed at 500 nM for both cell lines. Since the main entry mechanism of LK-4-eGFP was ATP-dependent endocytosis at 100 nM but ATP-independent penetration at 500 nM, we hypothesized that HSPG may be an important mediator for rapid induction of endocytosis in multimeric CPPs internalization at low concentrations, but not for direct penetration at high concentrations.

In order to support this hypothesis, we measured the relative affinity of LK-eGFPs on heparin, which mimics heparin sulfate in HSPG, by using biolayer interferometry.[25] The increase in the binding affinity in heparin was in accord with the increase of the degree of LK multimerization (Figure 10). The enhanced binding of LK multimers may have the potential to rapidly induce ATP-dependent endocytosis, mainly macropinocytosis. Interestingly, although the association rates of all LK-eGFPs did not show much difference from each other, the dissociation rates of LK-2- and LK-4-eGFPs were significantly

slower than LK-1- and LK-3-eGFPs. It is thought that even-numbered multimeric LK sequences have a tendency to bind to HSPG more effectively than odd-numbered sequences through rather specific interactions that take place beyond the electrostatic interaction.

Furthermore, we inhibited the attachment of heparan sulfate chains to HSPG using a xylosyltransferase-I (XylT-I) siRNA treatment on HeLa cells.[26] The rapid internalization of LK-4-eGFP within 30 min at 100 nM was reduced from 60% to 35% (Figure 11A). However, the inhibition was almost negligible at 500 nM. In addition, we compared the penetrating activities of LK-4-eGFPs on HEK 293T and HEK293s GnTI$^-$ cells. HEK293s GnTI$^-$ cells lack *N*-acetylglucosaminyltransferase I (GnTI), another key enzyme for the elongation of complex polysaccharide chains on HSPG.[27] The lack of GnTI clearly reduced the penetrating activity at 100 nM (Figure 11B). Additional XylT-I siRNA treatment on HEK293s GnTI$^-$ cells further decreased the penetrating activity. Again, the inhibitory effect on penetration activities was lowered by increasing the concentrations, and not observed at all at 500 nM. These results strongly support the hypothesis that the rapid internalization of multimeric CPPs are dependent upon HSPG at low concentrations, but not at high concentrations.

Using the data in the mechanism study, we proposed the internalization mechanisms of LK-fused proteins (Figure 12). The monomeric LK sequence with cationic charges has affinity with the negatively charged heparan sulfate chains of proteoglycan receptors on the plasma membrane, but this affinity is insufficient enough to induce endocytosis at nanomolar concentrations in a short period. Either a longer time (> 6 h) or a higher concentration (> 1 μM) is required to initiate endocytosis. However, the multimerization greatly enhances the affinity with heparan sulfate, and multimeric LK sequences can effectively initiate endocytosis within 0.5–1 h even at concentrations below 50 nM through the mediation of HSPG although the detailed mediating process is not yet understood. However, the multimeric LK sequences can interact directly with

the plasma membrane at concentrations over 500 nM, still much lower concentrations than the penetrating concentration of Tat (5 μM–10 μM), and can induce penetration without ATP consumption.

4.3. Control of adipocyte differentiation by LK multimer-fused transcription factor

The extraordinary cell penetrating activities of multimeric LK sequences enable biomacromolecules to rapidly penetrate cells at nanomolar concentrations. We believe that LK multimer-based delivery could be an effective solution to overcome the barrier of the plasma membrane severely prohibiting the intracellular biomedical effects of biomacromolecules at low concentrations. As a proof of concept, we intended to induce adipogenic differentiation though direct transcriptional control using an LK-4-fused transcription factor (Figure 13). The control of mesenchymal stem cell (MSC) differentiation has been of great interest to researchers and clinicians since it has the strong potential to be one of the key techniques for the development of future regenerative medicines.[28] Among MSC lineages, adipocytes play an essential role in maintaining whole-body energy homeostasis as part of an endocrine and paracrine organ although they are recognized as passive participants in the development of obesity.[29] Adipocyte differentiation involves a series of transcription factors to regulate temporal gene expression. According to the research that has been conducted so far, it is believed that PPAR-γ2 acts as the master transcription factor to induce adipocyte differentiation.[30] However, in most previous studies, adipocyte differentiation was induced either by combinatorial treatment of signaling molecules such as insulin, dexamethasone, and cAMP, or gene transfection in order to express the major transcription factors.[31] As far as we know, direct induction of adipogenesis via the transduction of transcription factors has never been tried. We examined the potency of LK-4-fused PPAR-γ2 to induce adipogenesis in 3T3-L1 cells. Pre-

adipocytes are recognized as the representative model in adipocyte differentiation.[32]

Firstly, we estimated the penetration of LK-4-fused proteins into 3T3-L1 cells using LK-4-eGFP. Although the penetration into 3T3-L1 cells was somewhat lower than into HeLa cells, more than 80% of cells were fluorescence-(+) cells at 200 nM (Figure 14A). The CLSM images also supported the efficient internalization of LK-4-eGFP into 3T3-L1 cells at nanomolar concentrations (Figure 14B). Most of the LK-4-eGFP was detected in the cytosol, but a small portion was clearly localized in the nucleus, where PPAR-γ2 plays a role in adipocyte differentiation.

LK-4-PPAR-γ2 was prepared by fusing LK-4 to the *N*-terminus of PPAR γ2 and purified though His-tag affinity chromatography and gel permeation chromatography (Figure 15A and 15B). LK-4-PPAR-γ2 was used to treat on 3T3-L1 cells every single day for adipocyte differentiation, and DPBS, LK-4-eGFP and PPAR-γ2 were used as controls. As shown in the optical microscopic images, the fibroblast-like polar morphology of the 3T3-L1 cells changed into adipocyte-like spherical morphology with intracellular lipid droplets after the LK-4-PPAR-γ2 treatment (Figure 16A and 16B). Oil Red O staining analysis showed the significant enhancement of lipid accumulation in a concentration-dependent manner following the treatment of LK-4-PPAR-γ2 (Figure 17A). At Day 9, the treatment of native PPAR-γ2 at a high concentration (1 μM) also showed a marginal increase (1.8-fold) in lipid accumulation. However, LK-4-PPAR-γ2 showed a higher lipid accumulation than native PPAR-γ2 even at 100 nM (2.2-fold). The induction of adipogenesis using LK-4-PPAR-γ2 was more dramatic when quantified by RT-PCR (Figure 17B and 17C). We measured the mRNA expression level of two PPAR-γ2 regulated genes, adiponectin and adipocyte protein 2 (aP2), and normalized them to a house-keeping gene, a non-POU domain-containing octamer-binding protein (NONO) gene.[33] At Day 9, native PPAR-γ2 showed only a 2-fold enhancement of adiponectin and aP2

expression at 1 μM, whereas LK-4-PPAR-γ2 showed 3-, 6-, and 55-fold enhancements of adiponectin and 3-, 6-, and 11-fold enhancements of aP2 at the concentrations of 100 nM, 200 nM, and 500 nM, respectively. The results strongly supported that LK-4-PPAR-γ is internalized into 3T3-L1 cells and can initiate the transcription of adipocyte-specific genes for differentiation into adipocyte cells.

The potential of our multimeric LK-4-mediated protein transduction for the adipocyte differentiation was compared with the conventional combinatorial treatment of insulin, dexamethasone, and isobutylmethylxanthin (IBMX) (Figure 18A and 18B). The induction of lipid accumulation by LK-4-PPAR-γ2 at 200 nM was slightly lower than the conventional method. However, the co-treatment of LK-4-PPAR-γ2 and sodium butyrate, a well-known histone deacetylase inhibitor to enhance transcription efficiency, could boost the lipid accumulation up to the level similar to the insulin-dexamethasone-IBMX method. We expected that more effective induction of adipogenic genes could be accomplished by future combinatorial treatment of transcription factors: for example, PPAR-γ, C/EPB, and Klf5, *etc*.[34]

5. Conclusion

We constructed a series of CPPs based on fusing multimeric α-helical amphiphatic LK sequences with cargo proteins. The fusion proteins can penetrate the cell membrane within 30 min at 100- to 1,000-fold lower concentrations than the penetrating concentrations of Tat-fused proteins. The multimeric CPP-fused proteins were internalized by ATP-dependent macropinocytosis through strong interactions with HSPG receptors at low nanomolar concentrations and through ATP-independent direct penetration at high nanomolar concentrations. Owing to the outstanding penetrating activities of the multimeric CPPs, we successfully delivered a transcription factor (PPAR-γ2) in an active form and induced adipogenesis at nanomolar concentrations. The discovery of multimeric CPPs may be a major breakthrough and could facilitate scientific studies on controlling intracellular biological reactions and the biomedical applications of delivering difficult therapeutic reagents into intracellular targets though rapid and efficient penetration at 2–3 orders of magnitude lower concentrations than standard CPPs.

6. References

1. (a) Gupta, B.; Levchenko, T. S.; Torchilin, V. P., Intracellular delivery of large molecules and small particles by cell-penetrating proteins and peptides. *Advanced drug delivery reviews* **2005,** *57* (4), 637-51; (b) Mae, M.; Langel, U., Cell-penetrating peptides as vectors for peptide, protein and oligonucleotide delivery. *Curr Opin Pharmacol* **2006,** *6* (5), 509-14; (c) Meade, B. R.; Dowdy, S. F., Enhancing the cellular uptake of siRNA duplexes following noncovalent packaging with protein transduction domain peptides. *Advanced drug delivery reviews* **2008,** *60* (4-5), 530-6.

2. (a) Thomas, C. E.; Ehrhardt, A.; Kay, M. A., Progress and problems with the use of viral vectors for gene therapy. *Nat Rev Genet* **2003,** *4* (5), 346-58; (b) Nayerossadat, N.; Maedeh, T.; Ali, P. A., Viral and nonviral delivery systems for gene delivery. *Advanced biomedical research* **2012,** *1*, 27.

3. Stone, D.; David, A.; Bolognani, F.; Lowenstein, P. R.; Castro, M. G., Viral vectors for gene delivery and gene therapy within the endocrine system. *The Journal of endocrinology* **2000,** *164* (2), 103-18.

4. Yin, H.; Kanasty, R. L.; Eltoukhy, A. A.; Vegas, A. J.; Dorkin, J. R.; Anderson, D. G., Non-viral vectors for gene-based therapy. *Nat Rev Genet* **2014,** *15* (8), 541-55.

5. (a) Koren, E.; Torchilin, V. P., Cell-penetrating peptides: breaking through to the other side. *Trends Mol Med* **2012,** *18* (7), 385-93; (b) Tiwari, G.; Tiwari, R.; Sriwastawa, B.; Bhati, L.; Pandey, S.; Pandey, P.; Bannerjee, S. K., Drug delivery systems: An updated review. *International journal of pharmaceutical investigation* **2012,** *2* (1), 2-11.

6. Guidotti, G.; Brambilla, L.; Rossi, D., Cell-Penetrating Peptides: From Basic Research to Clinics. *Trends Pharmacol Sci* **2017,** *38* (4), 406-424.

7. Frankel, A. D.; Pabo, C. O., Cellular uptake of the tat protein from human immunodeficiency virus. *Cell* **1988,** *55* (6), 1189-93.

8. Johnson, R. M.; Harrison, S. D.; Maclean, D., Therapeutic applications of cell-penetrating peptides. *Methods Mol Biol* **2011,** *683*, 535-51.

9. (a) Cheng, H.; Zhu, J. Y.; Xu, X. D.; Qiu, W. X.; Lei, Q.; Han, K.; Cheng, Y. J.; Zhang, X. Z., Activable Cell-Penetrating Peptide Conjugated Prodrug for Tumor Targeted Drug Delivery. *ACS Appl Mater Interfaces* **2015,** *7* (29), 16061-9; (b) Gros, E.; Deshayes, S.; Morris, M. C.; Aldrian-Herrada, G.; Depollier, J.; Heitz, F.; Divita, G., A non-covalent peptide-based strategy for protein and peptide nucleic acid transduction. *Biochim Biophys Acta* **2006,** *1758* (3), 384-93; (c) Meade, B. R.; Dowdy, S. F., Exogenous siRNA delivery using peptide transduction domains/cell penetrating peptides. *Advanced drug delivery reviews* **2007,** *59* (2-3), 134-40.

10. Khan, S.; Ullah, M. W.; Siddique, R.; Nabi, G.; Manan, S.; Yousaf, M.; Hou, H., Role of Recombinant DNA Technology to Improve Life. *Int J Genomics* **2016,** *2016*, 2405954.

11. (a) Dinca, A.; Chien, W. M.; Chin, M. T., Intracellular Delivery of Proteins with Cell-Penetrating Peptides for Therapeutic Uses in Human Disease. *Int J Mol Sci* **2016,** *17* (2), 263; (b) Munyendo, W. L.; Lv, H.; Benza-Ingoula, H.; Baraza, L. D.; Zhou, J., Cell penetrating peptides in the delivery of biopharmaceuticals. *Biomolecules* **2012,** *2* (2), 187-202.

12. Yamada, T.; Mehta, R. R.; Lekmine, F.; Christov, K.; King, M. L.; Majumdar, D.; Shilkaitis, A.; Green, A.; Bratescu, L.; Beattie, C. W.; Das Gupta, T. K., A peptide fragment of azurin induces a p53-mediated cell cycle arrest in human breast cancer cells. *Mol Cancer Ther* **2009,** *8* (10), 2947-58.

13. Kaitsuka, T.; Tomizawa, K., Cell-Penetrating Peptide as a Means of Directing the Differentiation of Induced-Pluripotent Stem Cells. *Int J Mol Sci* **2015,** *16* (11), 26667-76.

14. Duchardt, F.; Fotin-Mleczek, M.; Schwarz, H.; Fischer, R.; Brock, R., A comprehensive model for the cellular uptake of cationic cell-penetrating peptides. *Traffic* **2007,** *8* (7), 848-66.

15. (a) Jang, S.; Hyun, S.; Kim, S.; Lee, S.; Lee, I. S.; Baba, M.; Lee, Y.; Yu, J., Cell-penetrating, dimeric alpha-helical peptides: nanomolar inhibitors of HIV-1 transcription. *Angew Chem Int Ed Engl* **2014,** *53* (38), 10086-9; (b) Hyun, S.; Na, J.; Lee, S. J.; Park, S.; Yu, J., RNA Grooves Can Accommodate Disulfide-Bridged Bundles of a-Helical Peptides. *Chembiochem* **2010,** *11* (6), 767-770.
16. (a) Lupas, A. N.; Gruber, M., The structure of alpha-helical coiled coils. *Adv Protein Chem* **2005,** *70*, 37-78; (b) McAlinden, A.; Smith, T. A.; Sandell, L. J.; Ficheux, D.; Parry, D. A.; Hulmes, D. J., Alpha-helical coiled-coil oligomerization domains are almost ubiquitous in the collagen superfamily. *The Journal of biological chemistry* **2003,** *278* (43), 42200-7.
17. (a) Nagi, A. D.; Regan, L., An inverse correlation between loop length and stability in a four-helix-bundle protein. *Folding and Design* **1997,** *2* (1), 67-75; (b) Chen, X.; Zaro, J. L.; Shen, W. C., Fusion protein linkers: property, design and functionality. *Advanced drug delivery reviews* **2013,** *65* (10), 1357-69.
18. Madani, F.; Lindberg, S.; Langel, U.; Futaki, S.; Graslund, A., Mechanisms of cellular uptake of cell-penetrating peptides. *J Biophys* **2011,** *2011*, 414729.
19. (a) Jones, A. T., Macropinocytosis: searching for an endocytic identity and role in the uptake of cell penetrating peptides. *Journal of cellular and molecular medicine* **2007,** *11* (4), 670-84; (b) Mayor, S.; Pagano, R. E., Pathways of clathrin-independent endocytosis. *Nat Rev Mol Cell Biol* **2007,** *8* (8), 603-12; (c) Palm-Apergi, C.; Lonn, P.; Dowdy, S. F., Do cell-penetrating peptides actually "penetrate" cellular membranes? *Mol Ther* **2012,** *20* (4), 695-7.
20. (a) Di Pisa, M.; Chassaing, G.; Swiecicki, J. M., Translocation mechanism(s) of cell-penetrating peptides: biophysical studies using artificial membrane bilayers. *Biochemistry* **2015,** *54* (2), 194-207; (b) Walrant, A.; Bechara, C.; Alves, I. D.; Sagan, S., Molecular partners for interaction and cell internalization of cell-penetrating peptides: how identical are they? *Nanomedicine (Lond)* **2012,** *7* (1), 133-43.
21. (a) Chao, T. Y.; Raines, R. T., Mechanism of ribonuclease A endocytosis:

analogies to cell-penetrating peptides. *Biochemistry* **2011,** *50* (39), 8374-82; (b) Hallbrink, M.; Oehlke, J.; Papsdorf, G.; Bienert, M., Uptake of cell-penetrating peptides is dependent on peptide-to-cell ratio rather than on peptide concentration. *Biochim Biophys Acta* **2004,** *1667* (2), 222-8; (c) Jiao, C. Y.; Delaroche, D.; Burlina, F.; Alves, I. D.; Chassaing, G.; Sagan, S., Translocation and endocytosis for cell-penetrating peptide internalization. *The Journal of biological chemistry* **2009,** *284* (49), 33957-65; (d) Kuner, R., Central mechanisms of pathological pain. *Nat Med* **2010,** *16* (11), 1258-66.

22. (a) Christianson, H. C.; Belting, M., Heparan sulfate proteoglycan as a cell-surface endocytosis receptor. *Matrix Biol* **2014,** *35*, 51-5; (b) Koller, D.; Lohner, K., The role of spontaneous lipid curvature in the interaction of interfacially active peptides with membranes. *Biochim Biophys Acta* **2014,** *1838* (9), 2250-9; (c) Sarrazin, S.; Lamanna, W. C.; Esko, J. D., Heparan sulfate proteoglycans. *Cold Spring Harb Perspect Biol* **2011,** *3* (7).

23. Damiens, E.; El Yazidi, I.; Mazurier, J.; Elass-Rochard, E.; Duthille, I.; Spik, G.; Boilly-Marer, Y., Role of heparan sulphate proteoglycans in the regulation of human lactoferrin binding and activity in the MDA-MB-231 breast cancer cell line. *European Journal of Cell Biology* **1998,** *77* (4), 344-351.

24. (a) Xu, X.; Nagarajan, H.; Lewis, N. E.; Pan, S.; Cai, Z.; Liu, X.; Chen, W.; Xie, M.; Wang, W.; Hammond, S.; Andersen, M. R.; Neff, N.; Passarelli, B.; Koh, W.; Fan, H. C.; Wang, J.; Gui, Y.; Lee, K. H.; Betenbaugh, M. J.; Quake, S. R.; Famili, I.; Palsson, B. O.; Wang, J., The genomic sequence of the Chinese hamster ovary (CHO)-K1 cell line. *Nat Biotechnol* **2011,** *29* (8), 735-41; (b) Zhang, L.; Lawrence, R.; Frazier, B. A.; Esko, J. D., CHO Glycosylation Mutants: Proteoglycans. **2006,** *416*, 205-221.

25. Cheong, H. Y.; Groner, M.; Hong, K.; Lynch, B.; Hollingsworth, W. R.; Polonskaya, Z.; Rhee, J. K.; Baksh, M. M.; Finn, M. G.; Gale, A. J.; Udit, A. K., Heparin Binding to an Engineered Virus-like Nanoparticle Antagonist. *Biomacromolecules* **2017**.

26. Abu-Rub, M. T.; Newland, B.; Naughton, M.; Wang, W.; McMahon, S.; Pandit, A., Non-viral xylosyltransferase-1 siRNA delivery as an effective alternative to chondroitinase in an in vitro model of reactive astrocytes. *Neuroscience* **2016,** *339*, 267-275.

27. Chaudhary, S.; Pak, J. E.; Gruswitz, F.; Sharma, V.; Stroud, R. M., Overexpressing human membrane proteins in stably transfected and clonal human embryonic kidney 293S cells. *Nat Protoc* **2012,** *7* (3), 453-66.

28. (a) Baksh, D.; Song, L.; Tuan, R. S., Adult mesenchymal stem cells: characterization, differentiation, and application in cell and gene therapy. *Journal of cellular and molecular medicine* **2004,** *8* (3), 301-16; (b) Kim, N.; Cho, S. G., Clinical applications of mesenchymal stem cells. *The Korean journal of internal medicine* **2013,** *28* (4), 387-402.

29. (a) Lau, D. C.; Dhillon, B.; Yan, H.; Szmitko, P. E.; Verma, S., Adipokines: molecular links between obesity and atheroslcerosis. *Am J Physiol Heart Circ Physiol* **2005,** *288* (5), H2031-41; (b) Rosen, E. D.; Spiegelman, B. M., Adipocytes as regulators of energy balance and glucose homeostasis. *Nature* **2006,** *444* (7121), 847-53.

30. (a) Moseti, D.; Regassa, A.; Kim, W. K., Molecular Regulation of Adipogenesis and Potential Anti-Adipogenic Bioactive Molecules. *Int J Mol Sci* **2016,** *17* (1); (b) Rosen, E. D.; MacDougald, O. A., Adipocyte differentiation from the inside out. *Nat Rev Mol Cell Biol* **2006,** *7* (12), 885-96.

31. Farmer, S. R., Transcriptional control of adipocyte formation. *Cell Metab* **2006,** *4* (4), 263-73.

32. Zebisch, K.; Voigt, V.; Wabitsch, M.; Brandsch, M., Protocol for effective differentiation of 3T3-L1 cells to adipocytes. *Anal Biochem* **2012,** *425* (1), 88-90.

33. (a) Arsenijevic, T.; Gregoire, F.; Delforge, V.; Delporte, C.; Perret, J., Murine 3T3-L1 adipocyte cell differentiation model: validated reference genes for qPCR gene expression analysis. *PLoS One* **2012,** *7* (5), e37517; (b) Bai, P.;

Houten, S. M.; Huber, A.; Schreiber, V.; Watanabe, M.; Kiss, B.; de Murcia, G.; Auwerx, J.; Menissier-de Murcia, J., Poly(ADP-ribose) polymerase-2 [corrected] controls adipocyte differentiation and adipose tissue function through the regulation of the activity of the retinoid X receptor/peroxisome proliferator-activated receptor-gamma [corrected] heterodimer. *The Journal of biological chemistry* **2007,** *282* (52), 37738-46.

34. (a) Lee, J.-E.; Ge, K., Transcriptional and epigenetic regulation of PPARγ expression during adipogenesis. *Cell & Bioscience* **2014,** *4* (1), 29; (b) Lefterova, M. I.; Lazar, M. A., New developments in adipogenesis. *Trends in Endocrinology & Metabolism* **2009,** *20* (3), 107-114; (c) Siersbæk, R.; Nielsen, R.; Mandrup, S., Transcriptional networks and chromatin remodeling controlling adipogenesis. *Trends in Endocrinology & Metabolism* **2012,** *23* (2), 56-64; (d) Wang, L.; Waltenberger, B.; Pferschy-Wenzig, E.-M.; Blunder, M.; Liu, X.; Malainer, C.; Blazevic, T.; Schwaiger, S.; Rollinger, J. M.; Heiss, E. H.; Schuster, D.; Kopp, B.; Bauer, R.; Stuppner, H.; Dirsch, V. M.; Atanasov, A. G., Natural product agonists of peroxisome proliferator-activated receptor gamma (PPARγ): a review. *Biochemical Pharmacology* **2014,** *92* (1), 73-89; (e) Lee, J. E.; Ge, K., Transcriptional and epigenetic regulation of PPARgamma expression during adipogenesis. *Cell & bioscience* **2014,** *4*, 29; (f) Lefterova, M. I.; Lazar, M. A., New developments in adipogenesis. *Trends in endocrinology and metabolism: TEM* **2009,** *20* (3), 107-14; (g) Siersbaek, R.; Nielsen, R.; Mandrup, S., Transcriptional networks and chromatin remodeling controlling adipogenesis. *Trends in endocrinology and metabolism: TEM* **2012,** *23* (2), 56-64; (h) Wang, L.; Waltenberger, B.; Pferschy-Wenzig, E. M.; Blunder, M.; Liu, X.; Malainer, C.; Blazevic, T.; Schwaiger, S.; Rollinger, J. M.; Heiss, E. H.; Schuster, D.; Kopp, B.; Bauer, R.; Stuppner, H.; Dirsch, V. M.; Atanasov, A. G., Natural product agonists of peroxisome proliferator-activated receptor gamma (PPARgamma): a review. *Biochemical pharmacology* **2014,** *92* (1), 73-89.

35. Hyun, S.; Lee, S.; Kim, S.; Jang, S.; Yu, J.; Lee, Y., Apoptosis inducing, conformationally constrained, dimeric peptide analogs of KLA with submicromolar cell penetrating abilities. *Biomacromolecules* **2014,** *15* (10), 3746-52.

36. Omatsu-Kanbe, M.; Inoue, K.; Fujii, Y.; Yamamoto, T.; Isono, T.; Fujita, N.; Matsuura, H., Effect of ATP on preadipocyte migration and adipocyte differentiation by activating P2Y receptors in 3T3-L1 cells. *The Biochemical journal* **2006,** *393* (Pt 1), 171-80.

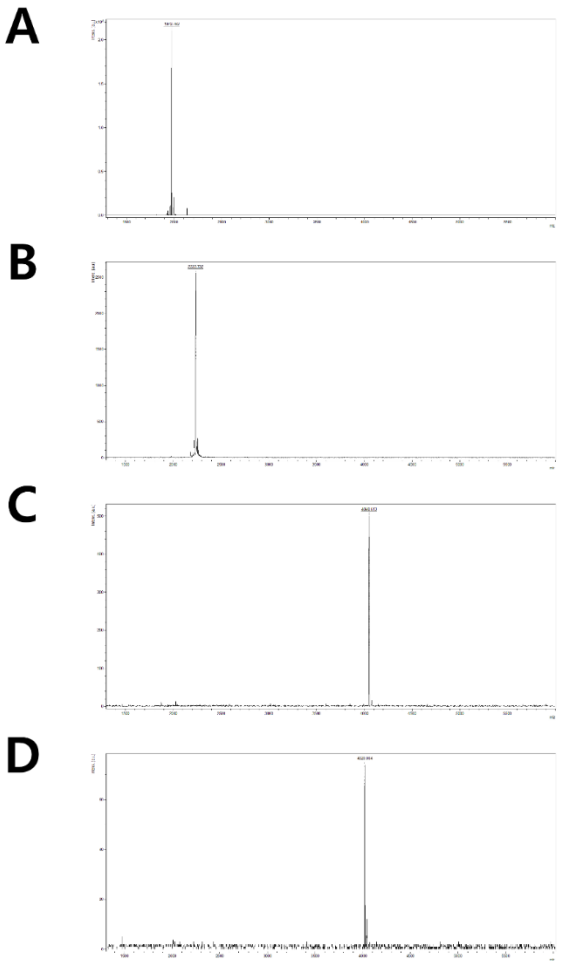

Figure 1. MALDI-TOF MS spectra of synthesized peptides. A) TAMRA-Tat. MS $[M+H]^+$: 1970.9 (calcd.), 1972.8 (found). B) TAMRA-LK-1. MS $[M+H]^+$: 2232.5 (calcd.), 2233.7 (found). C) TAMRA-LK dimer. MS $[M+H]^+$: 4049.5 (calcd.), 4048.5 (found). D) TAMRA-LK-2. MS $[M+H]^+$: 4020.9 (calcd.), 4020.0 (found).

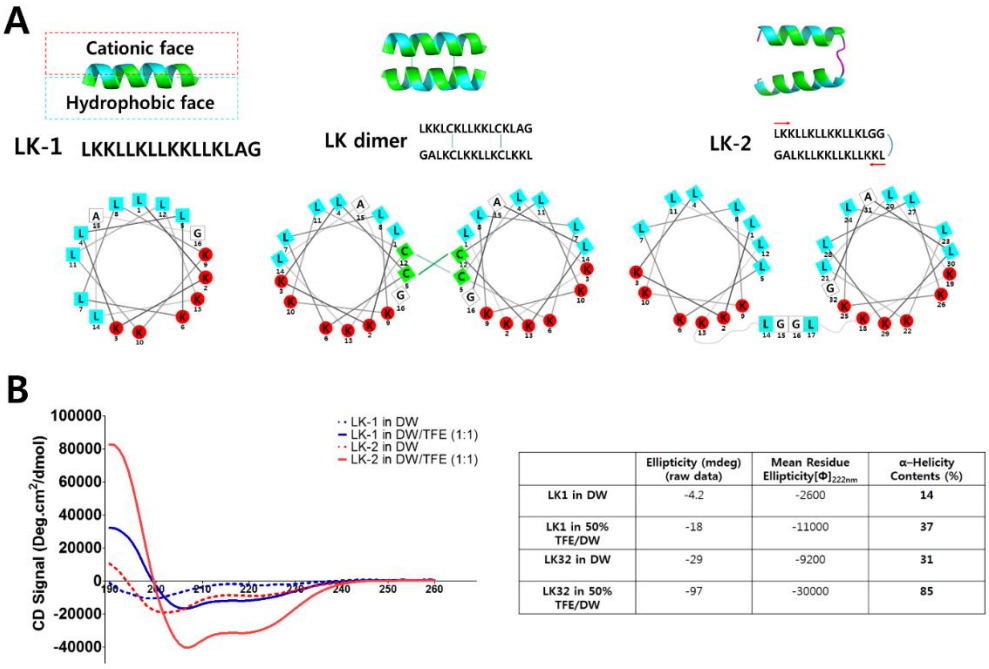

	Ellipticity (mdeg) (raw data)	Mean Residue Ellipticity[Θ]$_{222nm}$	α-Helicity Contents (%)
LK1 in DW	-4.2	-2600	14
LK1 in 50% TFE/DW	-18	-11000	37
LK32 in DW	-29	-9200	31
LK32 in 50% TFE/DW	-97	-30000	85

Figure 2. LK peptide and derivatives. A) Simplified sequences and structural representation of LK monomer (LK-1), LK dimer with two disulfide bonds, and LK-2. The structure of each peptide was predicted by PEP-FOLD (http://bioserv.rpbs.univ-paris-diderot.fr/services/PEP-FOLD/). B) Circular Dichroism (CD) of LK-1 and LK-2. CD spectra of LK-1 and LK-2 peptides in water and in 50% trifluoroethanol (TFE)/water mixture (left). Calculated α-helicities of LK-1 and LK-2(right). The CD was measured at the peptide concentration of 100 μM.

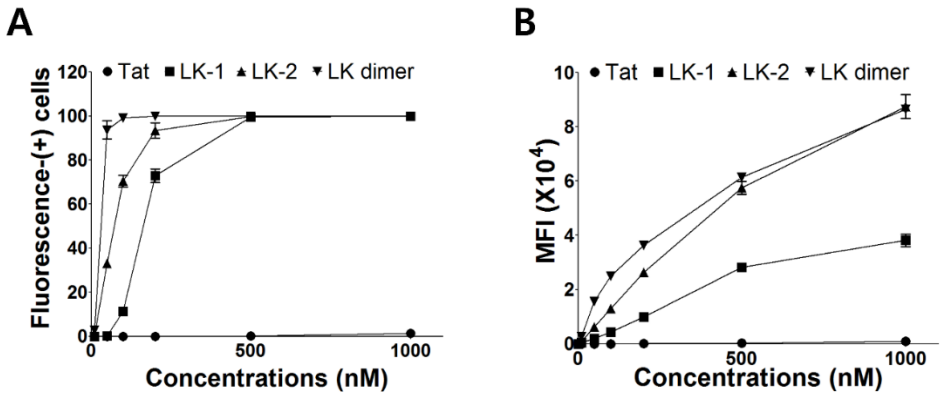

Figure 3. LK peptide and derivatives cell penetrating efficiency. A) Cell penetrating activities of TAMRA-labeled peptides on HeLa cells after 12 h-incubation. Fluorescence-(+) cells were analyzed by FACS. B) MFI means mean fluorescence intensity of cells in FACS data. Data points are represented as the average value of three experiments ± standard deviation.

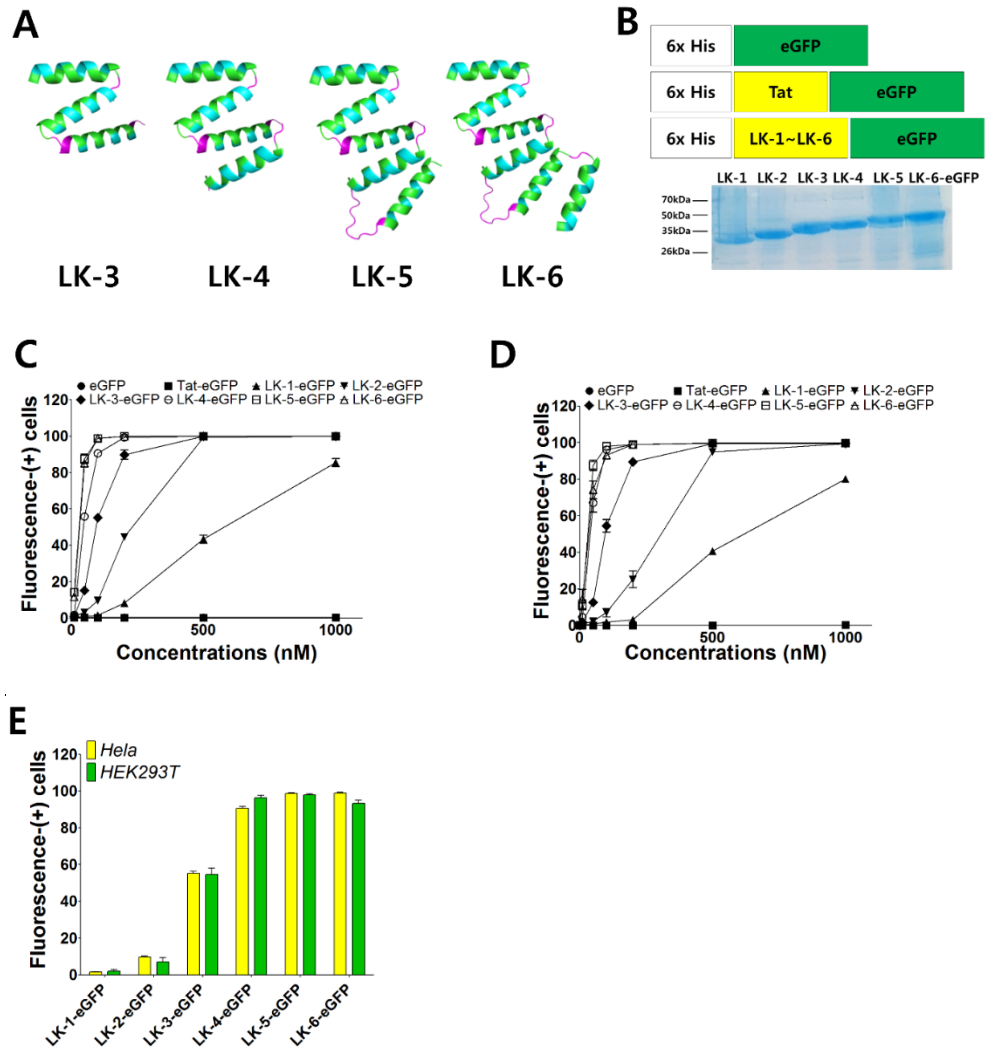

Figure 4. **Cell penetrating activity of LK-fused eGFP.** A) Schematic representation of LK-3, LK-4, LK-5, and LK-6 structures. The helix and HLH structure were predicted by PEP-FOLD. B) Construction of CPP-fused eGFP and the SDS-PAGE results of purified proteins. C) Cell penetration activities of CPP-fused eGFPs on HeLa cells after 12 h-incubation. Fluorescence-(+) cells were analyzed by FACS. D) Comparison of fluorescence-(+) cells on HeLa and HEK293T cells after 12 h-incubation with each CPP-fused eGFP at 100 nM. All data points are represented as the average value of three experiments ± standard deviation.

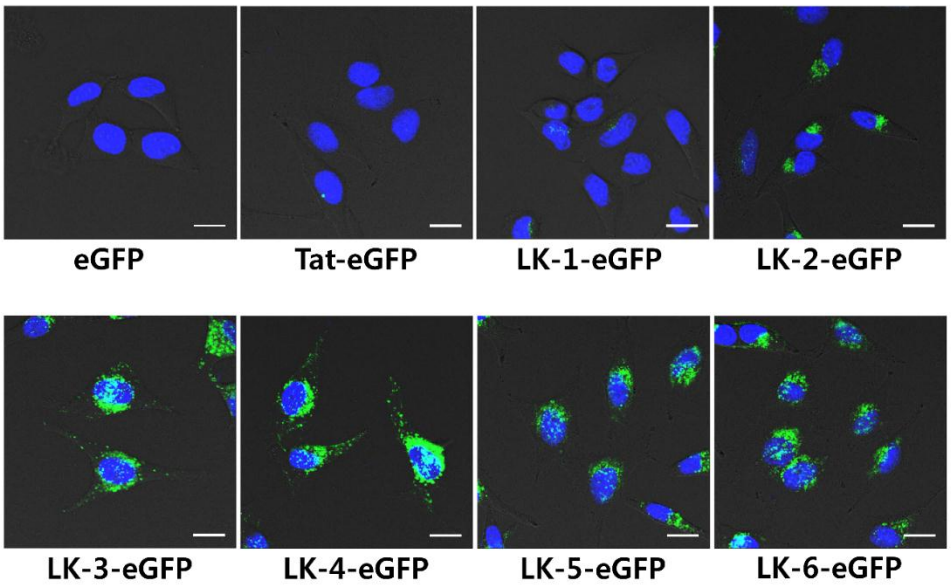

Figure 5. CLSM images of HeLa cells after 12 h- incubation with each CPP-fused eGFP at 100 nM. The intracellular localization of eGFPs was visualized as green and the Hoechst 33342-stained nucleus was shown as blue. The scale bar represents 20 μm.

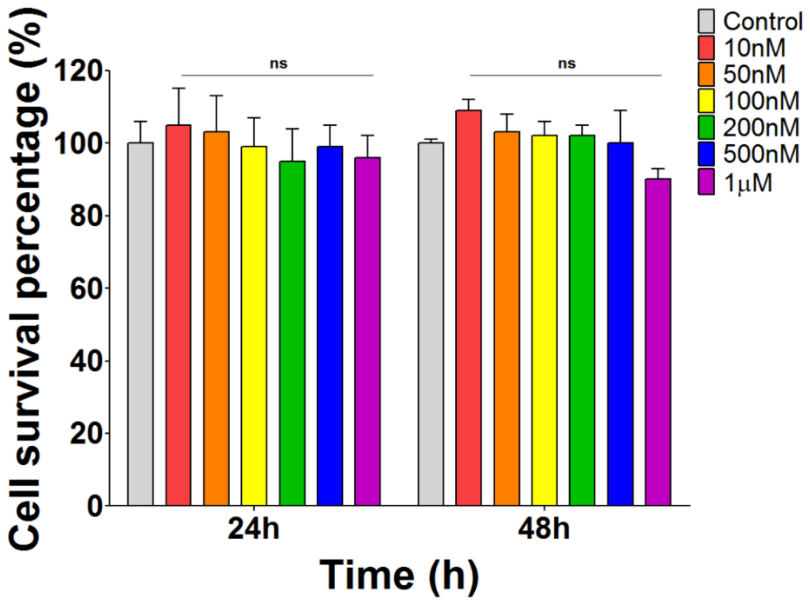

Figure 6. Relative viability of HeLa cells treated with LK-4-eGFP. HeLa cells were incubated with LK-4-eGFP at various concentrations for 24 h and 48 h. All data points are represented as the average value of three experiments ± standard deviation. The indication of 'ns' means that there was no significant difference with the control.

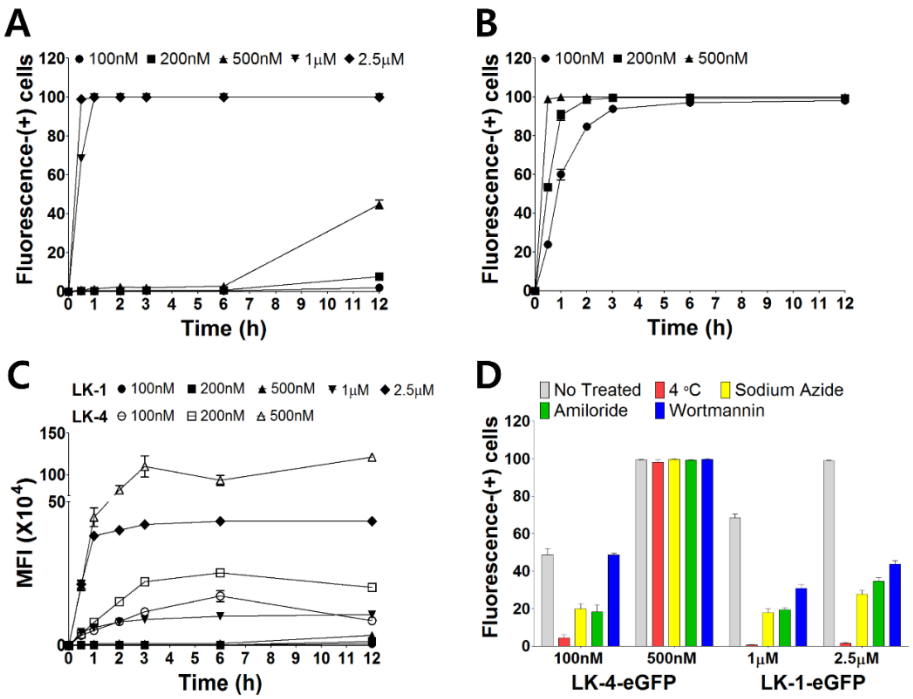

Figure 7. Cell penetrating kinetics and mechanism of LK multimers. Cell penetrating kinetics of A) LK-1-eGFP and B) LK-4-eGFP on HeLa cells at various concentrations. C) Cell penetrating kinetics of LK-1-eGFP and LK-4-eGFP on HeLa cells at various concentrations. FACS data were represented as mean fluorescence intensity (MFI). D) Inhibition of penetration of LK-1-eGFP and LK-4-eGFP into HeLa cells. Cells were pretreated with various inhibitory conditions for 1 h (4°C) or 3 h (others), and further incubated with LK-eGFPs at 37°C for 1 h. All data points are represented as the average value of three experiments ± standard deviation.

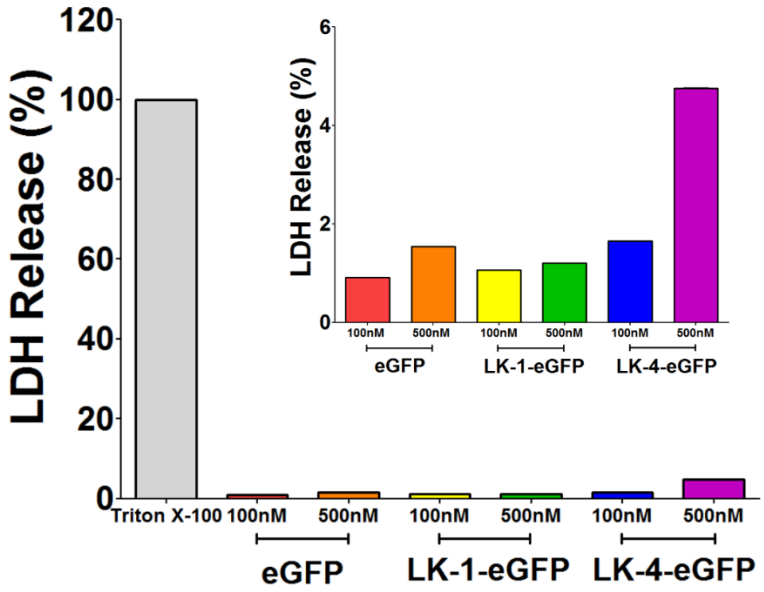

Figure 8. Membrane destabilization by LK-eGFPs. The LDH assay results on HeLa cells treated with LK-1-eGFP and LK-4 eGFP for 24 h. All data points are represented as the average value of three experiments ± standard deviation.

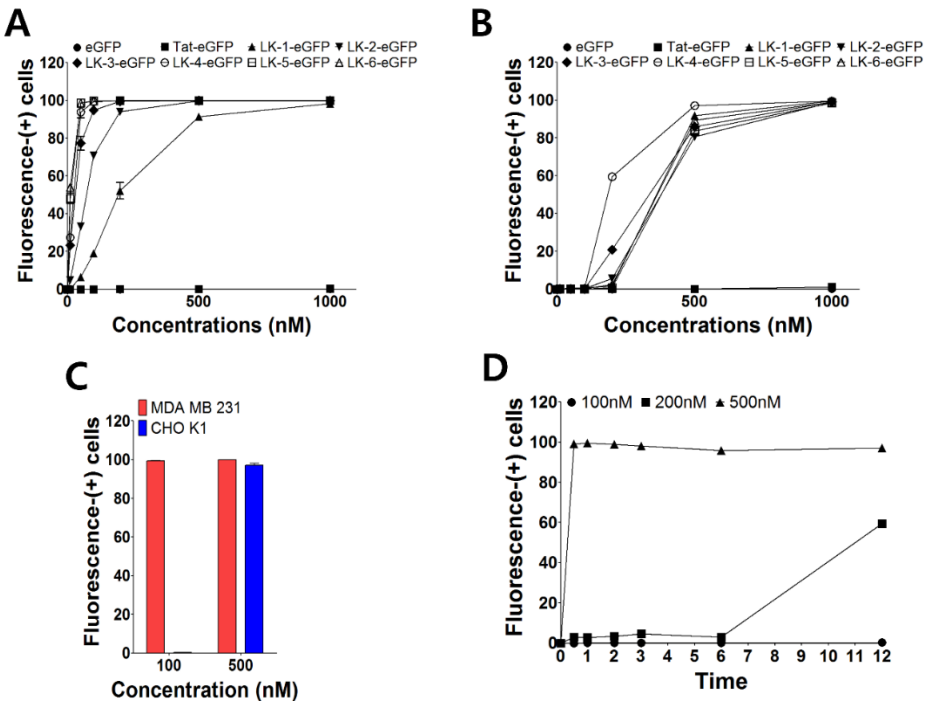

Figure 9. Effect of heparin sulfate on the entry of LK-fused eGFPs. A) Cell penetration activities of CPP-fused eGFPs on MDA-MB-231 B) Cell penetration activities of CPP-fused eGFPs on CHO-K1 cells after 12 h-incubation. C) Comparison of fluorescence-(+) cells on MDA-MB-231 and CHO-K1 cells after 12 h-incubation with LK-1-eGFP and LK-4-eGFP at 100 nM and 500 nM. D) Cell penetrating kinetics of LK-4-eGFP on CHO-K1 cells at various concentrations. All data points are represented as the average value of three experiments ± standard deviation.

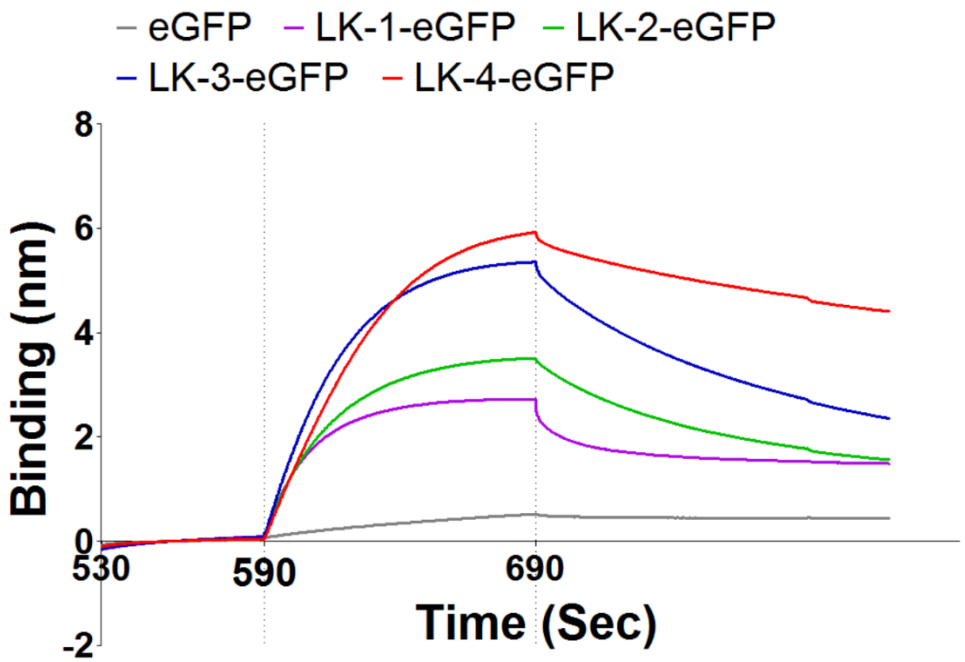

Figure 10. Biolayer interferometry measurement of LK-fused proteins. Comparison of the association and dissociation between LK-fused proteins (2.5 μM) and heparin which was measured by biolayer interferometry. eGFP (20 μM) was used as a control.

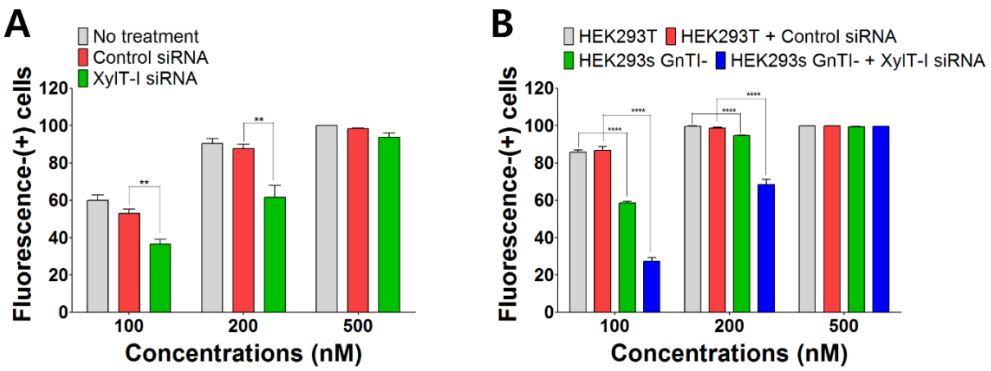

Figure 11. Effect of heparin sulfate on the entry of LK-fused eGFPs by knock-dwon XylT-I. A) Comparison of fluorescence-(+) cells on HeLa cells by siRNA-based inhibition of xylosyltransferase-I (XylT-I) expression. Cells were transfected by XylT-I siRNA for 48 h and then treated with LK-4-eGFP for 1 h. B) Comparison of fluorescence-(+) cells on HEK 293 cell lines by siRNA-based inhibition. HEK 293T and HEK293s GnTi$^-$ cells were transfected by control siRNA and XylT-I siRNA for 48 h and then treated with LK-4-eGFP for 0.5 h. Fluorescence-(+) cells were analyzed by FACS. All data points are represented as the average value of three experiments ± standard deviation. (**) and (***) indicate $0.001 \leq p < 0.01$ and $0.0001 \leq p < 0.001$, respectively.

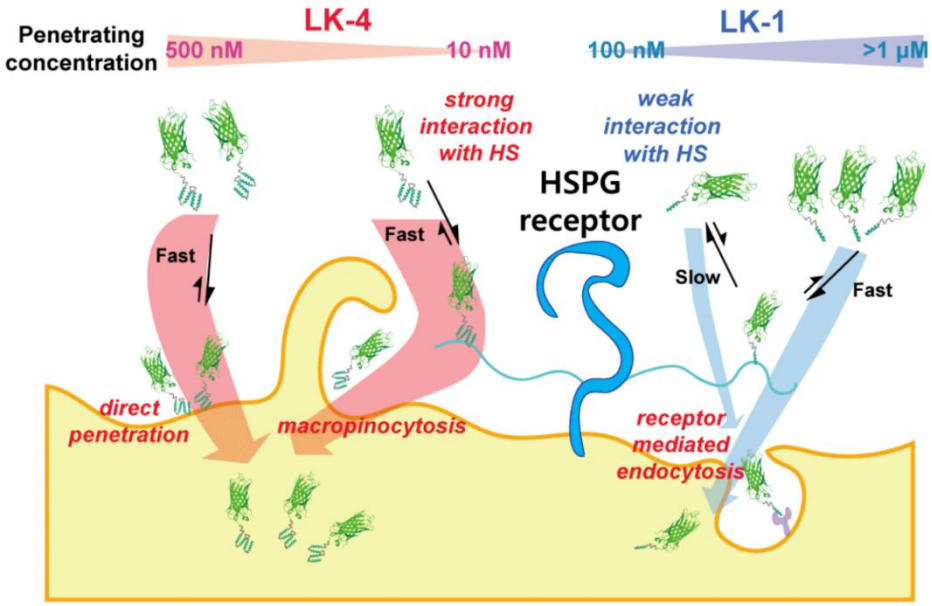

Figure 12. Proposed cell penetrating mechanisms of LK-1-eGFP and LK-4-eGFP.

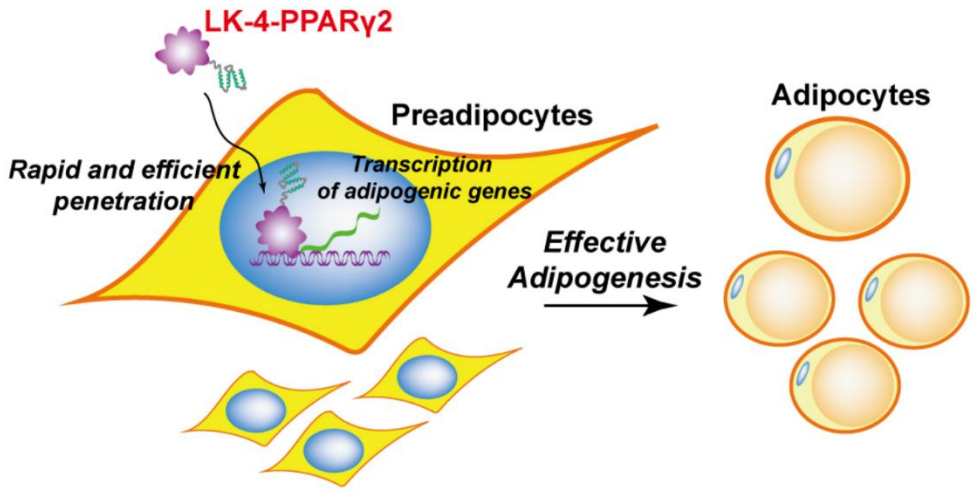

Figure 13. Schematic representation of induction of adipogenic gene expression by cell permeable LK-4-PPAR-γ2.

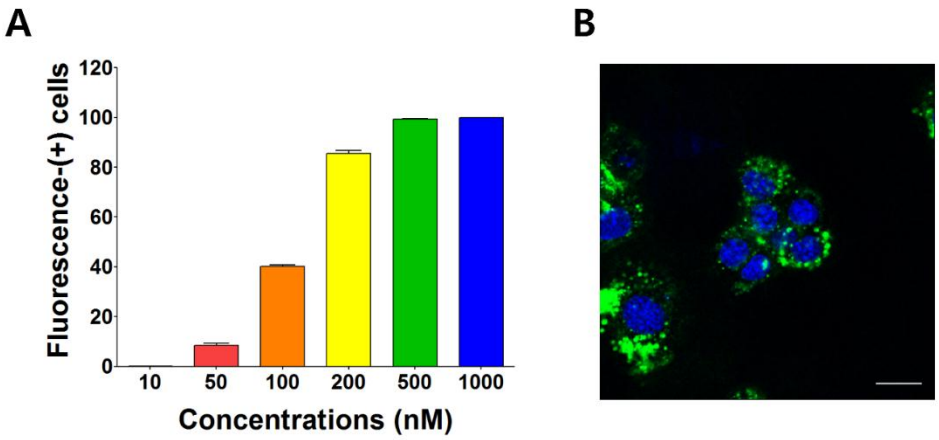

Figure 14. Penetrating activity in pre-adipocyte cells 3T3-L1 A) Cell penetration activities of LK-4-eGFPs on 3T3-L1 cells after 12 h-incubation. Fluorescence-(+) cells were analyzed by FACS. All data points are represented as the average value of three experiments ± standard deviation. B) A CLSM image of differentiated 3T3-L1 cells after 12 h-incubation with LK-4-eGFP at 200 nM. The nucleus was stained by Hoechst 33342 (blue). The scale bar represents 20 μm.

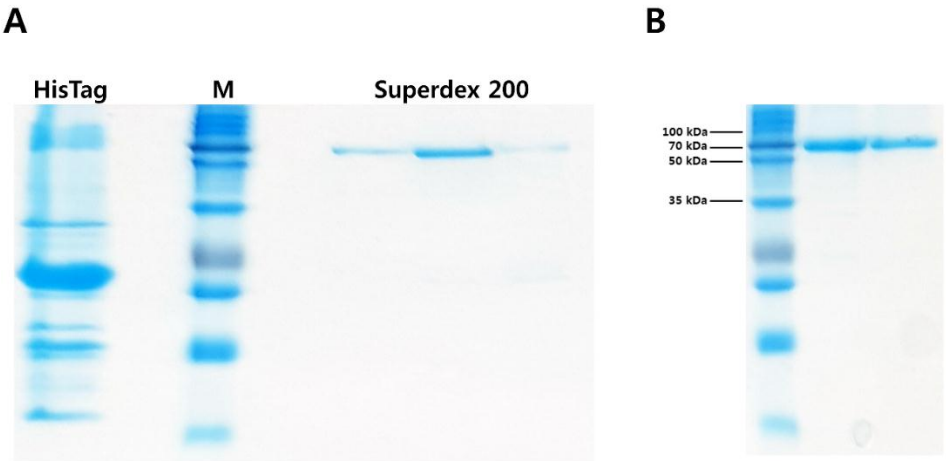

Figure 15. Purification of LK-4-PPAR-γ2 and PPAR-γ2. A) Proteins were initially purified from with a Ni-NTA column (left). Next, the protein mixture was further purified with a Superdex200 size column (right). B) The SDS-PAGE results of purified PPAR-γ2 and LK-4-PPAR-γ2.

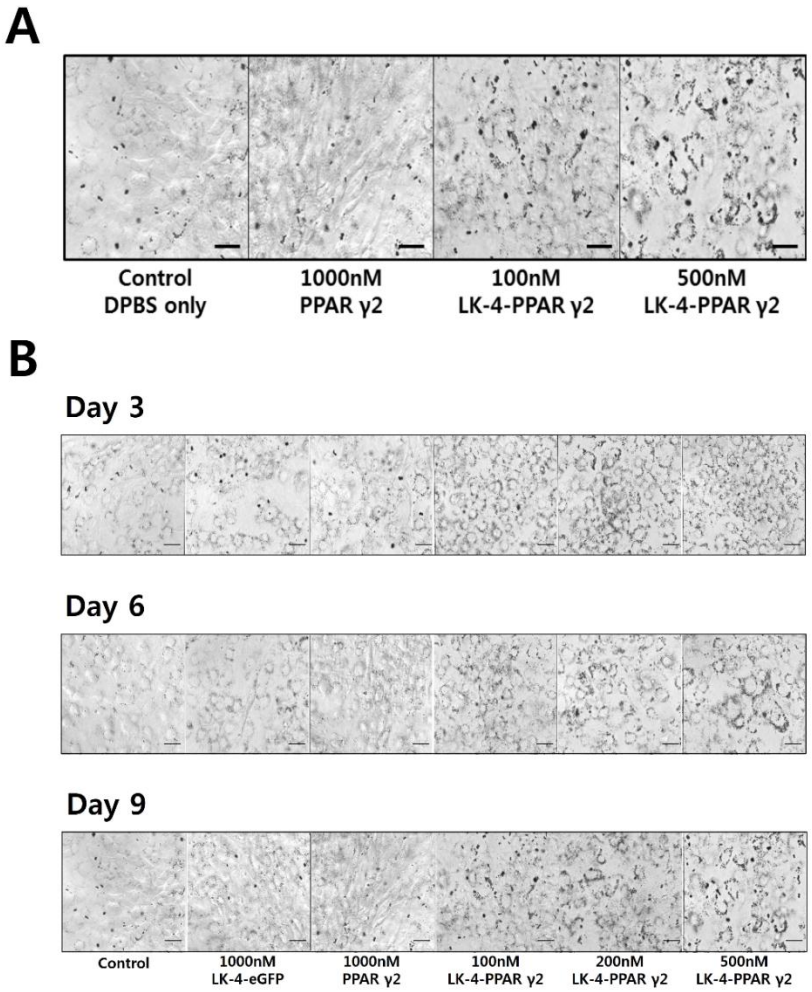

Figure 16. Adipocyte differentiation by LK-4-PPAR-γ2. A) Optical microscopic images of Oil O Red-stained 3T3-L1 cells treated with PPAR-γ2 and LK-4-PPAR-γ2 at Day 9. DPBS was used for control and proteins were added to the cells every single day from Day 0 to Day 8. The scale bar represents 40 μm. F) DPBS was used for control and proteins were added to the cells every single day from Day 0 to Day 8. The scale bar represents 40 μm.

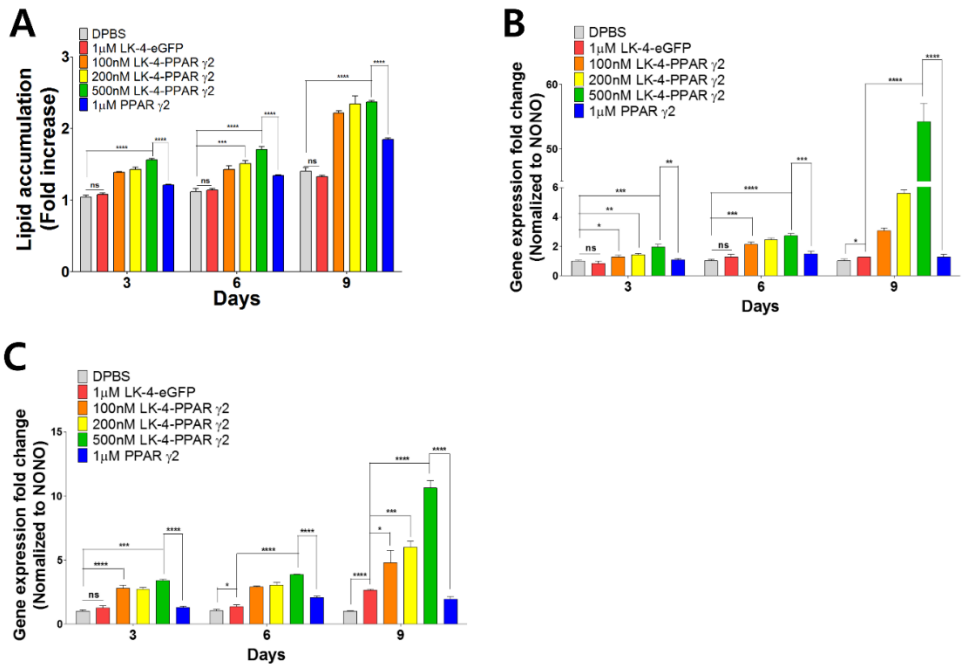

Figure 17. Induction of adipogenic gene expression by LK-4-PPAR-γ2. A) Quantitative measurement of Oil O Red accumulated in differentiated 3T3-L1 cells. The Oil O Red was extracted with isopropanol and quantified at 540 nm. Relative mRNA levels of B) adiponectin and C) aP2 genes in differentiated 3T3-L1 cells treated with PPAR-γ2 and LK-4-PPAR-γ2 every single day from Day 0 to Day 8. The mRNA expression was quantified by RT-PCR. Each value was normalized to NONO gene expression. All data points are represented as the average value of three experiments ± standard deviation. (*), (**), (***), and (****) indicate $0.01 \leq p < 0.05$, $0.001 \leq p < 0.01$, $0.0001 \leq p < 0.001$ and $p < 0.0001$, respectively. The indication of 'ns' means that there was no significant difference.

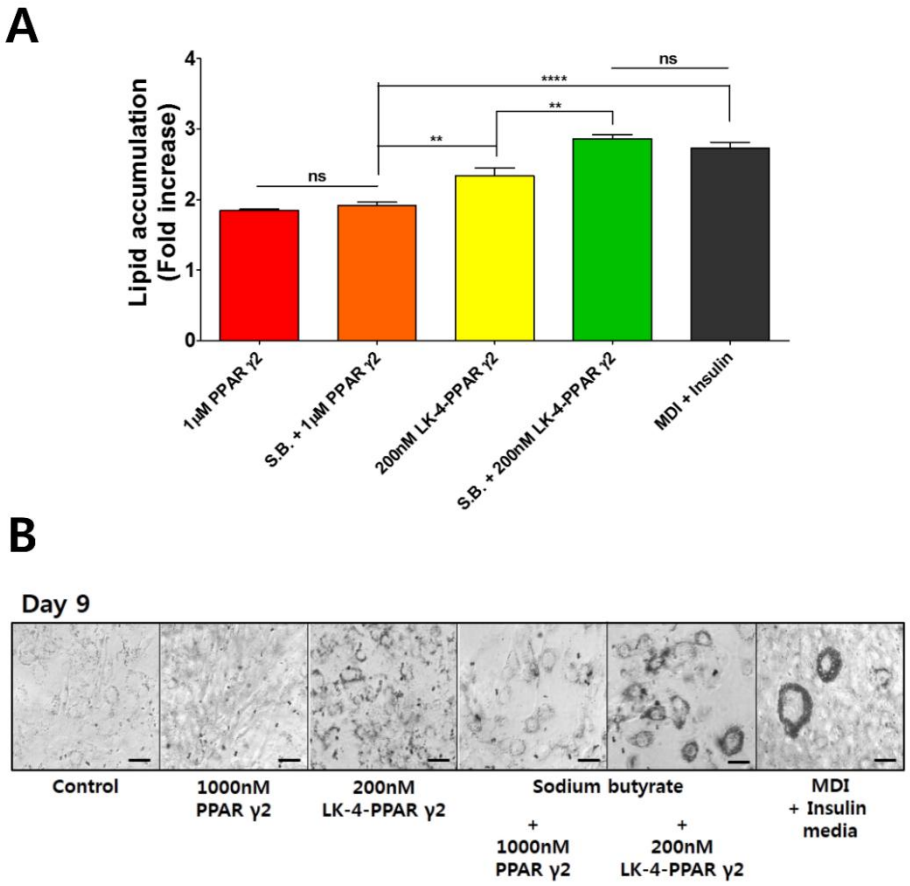

Figure 18. Comparison of adipocyte differentiation efficiency with the MDI method. A) Quantitative measurement of Oil O Red accumulated in differentiated 3T3-L1 cells at Day 9. The Oil O Red was extracted with isopropanol and quantified at 540 nm. All data points are represented as the average value of three experiments ± standard deviation. (**) and (****) indicate $0.001 \leq p < 0.01$ and $p < 0.0001$, respectively. The indication of 'ns' means that there was no significant difference. B) Optical microscopic images of Oil O Red-stained 3T3-L1 cells at Day 9. The scale bar represents 40 μm. S.B. and MDI represent sodium butyrate and methylisobutyxanthine/dexamethasone induction, respectively.

Gene constructs	Amplified gene	Primers (5′ to 3′)	Restriction Enzymes
pET28-eGFP	eGFP	For: CGCGGATCCGTGAGCAAGGGCGAG	BamHI
		Rev: GAGCTGTACAAGTAACTCGAGCAC	XhoI
pET28-Tat-eGFP	Tat	For: AGCCATATGTACGGCC	NdeI
		Rev: CCGTCGCGGATCCGTG	BamHI
pET28-LK-1-eGFP	LK-1	For: TCCGAATTCACTGAAGAAACT	EcoRI
		Rev: AACTGGCTGGTGGATCCGTG	BamHI
pET28-LK-2-eGFP	LK-2	For: AGCCATATGCTCAAGAAACTGC	NdeI
		Rev: GAAACTGGCTGGTGGATCCGTG	BamHI
pET28-LK-3-eGFP	LK-3	For: TCCGAATTCACTGAAGAAACT	EcoRI
		Rev: GAGCTGTACAAGTAACTCGAGCAC	XhoI
pET28-LK-4-eGFP	LK-4	For: TCCGAATTCCTCAAGAAACTGCTGAAG	EcoRI
		Rev: GAGCTGTACAAGTAACTCGAGCAC	XhoI
pET28-LK-5-eGFP	LK-5	For: TTCGAGCTCACTGAAGAAACTGCTCA	SacI
		Rev: GAGCTGTACAAGTAACTCGAGCAC	XhoI
pET28-LK-6-eGFP	LK-6	For: TTCGAGCTCACTCAAGAAACTGCTGA	SacI
		Rev: GAGCTGTACAAGTAACTCGAGCAC	XhoI
pET28-PPAR γ2	PPAR γ2	For: AGCCATATGATGGGTGAAACTCTGG	NdeI
		Rev:GTGCTCGAGTTAATACAAGTCCTTGTAGATCTCC	XhoI
pET28-LK-4 -PPAR γ2	LK-4	For: TAACTCGAGCACCACC	XhoI
		Rev:CATGAGCTCGGATCCACCAGCCAGTTTCAAC	SacI
pET28-LK-4 -PPAR γ2	PPAR γ2	For: TCCGAGCTCATGGGTGAAACTCTGGG	SacI
		Rev: GTGCTCGAGTTAATACAAGTCCTTGTAGATCTCC	XhoI

Table 1. Primer sequences for the recombinant DNA constructs.

RT qPCR target gene	Primers (5′ to 3′)
NONO (house keeping gene)	For: UGCUCCUGUGCCACCUGGUACUC
	Rev: CCGGAGCUGGACGGUUGAAUGC
aP_2	For: UGCCACAAGGAAAGUGGCAG
	Rev: CUUCACCUUCCUGUCGUCUG
Adiponectin	For: AAGAAGGACAAGGCCGUUCUCUU
	Rev: GCUAUGGGUAGUUGCAGUCAGUU

Table 2. Primer sequences for RT-qPCR.

LK Multimers	Amino acid sequences (Linker)
LK-3 (trimer)	LKKLLKLLKKLLKLGGLKKLLKLLKKLLKLAGGSEFLKKLLKLLKKLLKL AG
LK-4 (tetramer)	LKKLLKLLKKLLKLGGLKKLLKLLKKLLKLAGGSEFLKKLLKLLKKLLKL GGLKKLLKLLKKLLKLAG
LK-5 (pentamer)	LKKLLKLLKKLLKLGGLKKLLKLLKKLLKLAGGSEFLKKLLKLLKKLLKL GGLKKLLKLLKKLLKLAGKSSDPNSSSLKKLLKLLKKLLKLAG
LK-6 (hexamer)	LKKLLKLLKKLLKLGGLKKLLKLLKKLLKLAGGSEFLKKLLKLLKKLLKL GGLKKLLKLLKKLLKLAGKSSDPNSSSLKKLLKLLKKLLKLGGLKKLLK LLKKLLKLAG

Table 3. Amino acid sequences of multimeric LK peptides.

List of Publications

1. S Choi, **JH Oh**, H Kim, SH Nam, J Shin and JS Park. Protective Effect of Tat PTD-Hsp27 Fusion Protein on Tau Hyperphosphorylation Induced by Okadaic Acid in the Human Neuroblastoma Cell Line SH-SY5Y. Cell Mol. Neurobiol. 2015 Oct; 35(7):1049-59.

2. **JH Oh**, S Choi, J Shin and JS Park. Protective Effect of Recombinant Soluble Neprilysin Against β-Amyloid Induced Neurotoxicity. Biochem. Biophys. Res. Commun. 2016 Sep 2; 477(4):614-19.

3. H Kim, B Choi, H Lim, H Min, **JH Oh**, S Choi, JG Cho, JS Park and SJ Lee. Polyamidoamine Dendrimer-Conjugated Triamcinolone Acetonide Attenuates Nerve Injury-Induced Spinal Cord Microglia Activation and Mechanical Allodynia. Mol. Pain. 2017 Jan; 13:1-11.

4. GC Kim, JH Ahn, **JH Oh**, S Nam, S Hyun, J Yu and Y Lee. Photoswitching of Cell Penetration of Amphipathic Peptides by Control of α-Helical Conformation. Biomacromolecules. 2018 June, DOI: 10.1021/acs.biomac.8b00428.

5. **JH Oh**, SE Chong, S Nam, S Hyun, S Choi, H Gye, S Jang, J Jang SW Hwang, J Yu and Y Lee. Multimeric Amphipathic α-Helical Sequences for Rapid and Efficient Intracellular Protein Transport at Nanomolar Concentrations. Adv. Sci. 2018 June, DOI: 10.1002/advs.201800240.

Abstract in Korean (국문 초록)

작은 분자 (> 1 kDa) 및 유전자는 치료용 물질로써 다양한 치료 연구를 성공적으로 진행 할 수 있다. 그러나 작은 분자는 제한된 특이성 및 선택성으로 인하여 약물 효율성에 대한 부작용을 야기한다. 또한 유전자를 치료용 물질로 사용하는 것은 많은 경우에 안전성의 문제를 배제할 수 없다. 재조합 단백질은 이러한 한계를 극복하기 위한 대체 물질로 다양한 분야에 응용되고 있다. 재조합 단백질은 높은 특이성, 선택성, 안전성과 같은 장점을 가지고 있을 뿐 아니라 이것의 생산 과정 또한 매우 간단하고 체계적이다. 이 연구에서는 재조합 단백질을 알츠하이머 질병 (AD) 치료뿐 아니라 유용한 생물학적 적용에 필요한 물질을 전달하는 매개체로써 응용했다.

알츠하이머 질병은 뉴런을 손상시키고 기억, 학습 및 추론을 포함하는 뇌 기능의 상실을 유발하는 뇌세포 퇴행성 장애이다. 현재까지 알츠하이머 질병은 크게 두 가지 주요 병리학 적 특징을 보인다고 알려져 있다. 그 첫 번째는 뇌세포 내부와 외부에서의 아밀로이드 베타 (Aβ)의 축적이고 다른 하나는 뇌세포 내부에서의 타우 (Tau)의 과인산화를 통한 신경 내 신경원섬유엉킴 (NFTs) 이다. Part 1에서는 이 두 가지 특징에 대한 방어 또는 완화 효과를 기대하는 알츠하이머 질병의 치료제 개발을 하고자 하였다.

아밀로이드 베타의 축적은 소수성 아밀로이드 베타 펩타이드 (Aβ1−40 또는 Aβ1−42)로 인해 유발된다. 제 2형 세포막 결합 효소인 네프릴라이신 (NEP)은 아밀로이드 베타 펩타이드를 분해하는 주요 효소이다. 네프릴라이신 단백질은 아밀로이드 베타 펩타이드의 단량체 뿐 아니라 다량체 형태도 분해 할 수 있는 특성을 가

짐으로 다른 효소들 보다 더 알츠하이머 완화에 효과적일 것으로 기대하였다. 뇌세포의 독성을 유발하는 아밀로이드 베타 펩타이드를 분해하기 위해 세포막 결합 영역을 제거한 재조합 용해성 네프릴라이신 단백질 (sNEP)을 동물세포 (HEK293T)에서 생산하고 뇌세포에서 아밀로이드 베타 펩타이드에 대한 완화 효과를 입증하였다.

신경섬유엉킴은 미세관 관련 단백질 타우의 과인산화로 인한 응축으로 유발된다. 정상적인 타우 단백질은 미세관을 안정화하여 세포를 보호하는 반면 과인산화 된 타우는 뇌세포 내부의 미세관의 안정화를 어렵게 하고 단백질의 응축을 통해 세포사멸을 유발시킨다. 따라서 과인산화 된 타우의 수준을 감소시키는 것은 알츠하이머 질병 치료에 결정적 영향을 준다. 이전 연구에서 열 충격 단백질 (Hsp27)은 과인산화된 타우에 직접적 결합을 통해 타우 단백질을 효과적으로 제거한다는 것이 밝혀졌다. 이를 바탕으로 이 연구에서는 과인산화에 따른 알츠하이머 질병의 완화 효과를 위해 재조합 Hsp27 단백질을 사용하였다. Hsp27 단백질 자체는 세포 내의 투과성을 가지지 않기 때문에 세포 투과성 펩타이드 (Cell Penetrating Peptide, CPP)를 Hsp27에 융합하여 단백질에 세포 투과성을 부여하였다. 이 연구에서는 에이즈 바이러스 (HIV)에서 유래한 11개의 아미노산 서열 (YGRKKRRQRRR)로 이루어진 Tat 펩타이드를 세포 투과성 펩타이드로서 사용하였다. 세포 투과성을 가지는 Tat-Hsp27을 뇌세포에 처리함으로써 뇌세포내에서의 타우단백질 발현의 감소와 이를 통한 뇌세포 사멸의 완화 효과를 입증하였다.

Part 2에서는 단백질을 효율적으로 세포 내로 전달 할 수 있는 새로운 종류의 세포 투과성 펩타이드를 개발하는 연구를 진행하였다. 세포 투과성 펩타이드는 다양한 생물학적, 의학적 응용으로서 사용

된다. 하지만 대부분의 세포 투과성 펩타이드는 마이크로몰 농도 수준의 높은 세포 투과 농도 임계치를 가지며 이것은 세포 투과성 펩타이드의 광범위한 응용을 저해하는 중대한 약점을 야기한다.

이전 연구에서 16개의 양친매성 알파 나선형을 가지는 LK펩타이드 (amphipathic α-helical LK peptide)를 개발하였고 이는 나노몰 농도 수준의 세포 투과 농도임계치를 가지는 것으로 밝혀졌다. 또한 기존의 연구에서 LK 펩타이드의 세포 투과 활성은 LK의 이량체는 단량체보다 더 높은 세포 투과도를 가진다는 것도 밝혀졌다. 본 연구에서는 기존의 연구의 확장으로서 LK의 다량체의 제작을 통해 더욱 효과가 향상된 새로운 종류의 세포 투과성 펩타이드를 개발하였다. 더 나아가서 LK 펩타이드의 세포 투과 메커니즘을 규명하고 실질적인 생물학적 응용에 성공적으로 적용하였다.

주요어
재조합 단백질, 알츠하이머 질병, 열 충격 단백질 27 (Hsp27), 네프릴라이신 (NEP), 세포 투과성 펩타이드 (CPPs)

학번: 2013-22928